



DIPLOMARBEIT

Titel der Diplomarbeit

Structural and Functional Characterization of Chlorite Dismutases and Homologous Proteins

Andreas Hagmüller

angestrebter akademischer Grad

Magister der Naturwissenschaften (Mag.rer.nat.)

Wien, 2013

Studienkennzahl lt. Studienblatt:	A 490
Studienrichtung lt. Studienblatt:	Diplomstudium Molekulare Biologie
Betreuerin / Betreuer:	Univ.-Prof. Dipl.-Ing. Dr. Kristina Djinovic-Carugo

Index

1. Abstract
2. Zusammenfassung
3. Introduction
 - 3.1 Oxochlorates
 - 3.2 Chlorite Dismutase
 - 3.3 Structure of Chlorite Dismutase
 - 3.4 Reaction Mechanism
 - 3.5 Catalytically Important Residues
 - 3.6 Sources of Cld
 - 3.6.1 *Nitrospira defluvii*
 - 3.6.2 *Listeria monocytogenes*
 - 3.6.3 *Sulfolobus solfataricus*
4. Aim of this Thesis
5. Materials and Methods
 - 5.1 Media, Buffers and Stock Solutions
 - 5.2 Storage
 - 5.3 Cloning and Expression
 - 5.4 Expression Vectors
 - 5.5 Constructs
 - 5.6 Cloning
 - 5.7 Site Directed Mutagenesis
 - 5.8 Polymerase Chain Reaction
 - 5.9 Transformation
 - 5.10 Colony PCR
 - 5.11 Small Scale Plasmid Preparation
 - 5.12 Subcloning
 - 5.13 Protein Expression
 - 5.13.1 NdCld: wildtype and mutant expression
 - 5.13.2 NdCld: expression without heme
 - 5.13.3 LmCld
 - 5.13.4 SsCld
 - 5.13.5 NwCld
 - 5.14 Protein Purification
 - 5.15 Purification conditions
 - 5.15.1 Purification of NdCld wild type and mutants
 - 5.15.2 Purification of apoNdCld
 - 5.15.3 Purification of LmCld

- 5.15.4 Purification of NwCld
 - 5.16 Strep-Tactin Affinity
 - 5.17 Ni-NTA Affinity
 - 5.18 Further Purification
 - 5.19 Immuno-precipitation
 - 5.20 Heme-staining
 - 5.21 Fluorescence based Thermal Shift Assay
 - 5.22 Crystallography
 - 5.22.1 Robotics and Materials
 - 5.22.2 Crystallization of LmCld
 - 5.22.3 Crystallization of LmCld with Additives
 - 5.22.4 Crystallization of NdCld W145F
 - 5.23 Structure Determination
 - 5.23.1 Data Collection
 - 5.23.2 Molecular Replacement
 - 5.23.3 Refinement
 - 5.23.4 Localization of Anomalous Scatterers
 - 5.24 Steady-state Kinetics
 - 5.25 Static Light Scattering
 - 5.26 UV-vis Spectroscopy
- 6. Results
 - 6.1 Thermal Shift Assay
 - 6.2 Structure of recombinant LmCld
 - 6.3 Structure of LmCld with Protamine
 - 6.4 LmCld with Anomalous Scatterers
 - 6.5 Native LmCld
 - 6.5.1 Heme-staining of native LmCld
 - 6.5.2 X-Ray Fluorescence
 - 6.5.3 Inductively Coupled Plasma Mass Spectrometry
 - 6.5.4 Hydrophobic Cofactor Mass Spectrometry
 - 6.6 Structure of NdCld W145F
 - 6.7 Structure of NdCld W145F in Complex with Cyanide
 - 6.8 Oligomeric State of Different Clds
 - 6.9 Heme Content of SsCld
 - 6.10 Steady-state Kinetics
 - 6.11 Steady-state Kinetics of NdCld W145F
- 7. Discussion
- 8. References
- 9. List of Figures
- 10. List of Tables

- 11.Nomenclature
- 12.Acknowledgements
- 13.Curriculum Vitae

1. Abstract

The heme-enzyme chlorite dismutase (Cld) catalyzes the decomposition of chlorite to chloride and molecular oxygen. In (per-)chlorate respiring bacteria (PCRB), where it was first discovered, Cld degrades the toxic end product of the respiratory chain, thus evading self-toxicification. The enzyme and its homologues are found in several distinct bacterial and archaeal phyla with bioinformatics suggesting lateral gene transfer also between these two domains. Nonetheless most strains are not PCRBs, hence the physiological role of many Clds is not as obvious and many do not show chlorite degrading activity (Cld-like proteins). Since the chlorite contamination is a rather recent problem caused by industrial processes the question about the enzyme's original evolutionary purpose arises. Water contamination by chlorite has become a serious issue in the USA and bioremediation by Cld would present an efficient way to detoxify. Some human pathogens contain a *cld*-gene, including *Listeria monocytogenes*, whose gene-product appears to be essential, making it a potential drug target.

Attempts have been made to predict Cld-activity based on the sequence and several residues have been suggested to represent signature residues for active Clds. One part of this thesis will deal with mutation studies of these residues on the active Cld from *Nitrospira defluvii* (a non-PCRB) and the effect on the enzyme's kinetics.

The second part will focus on the search for the function of Cld from *Listeria monocytogenes* (LmCld). Preliminary work did not show evidence for heme-binding nor Cld-activity so the main focus is on finding another cofactor which might mediate another function.

The third part describes the initial work on Cld from *Sulfolobus solfataricus* (SsCld), a acido-thermophile archaeon, which lacks the key residue for Cld-activity but binds heme.

2. Zusammenfassung

Das Häm-bindende Enzym Chlorite Dismutase (Cld) katalysiert den Abbau von toxischem Chlorit zu Chlorid und O₂. In (Per)Chlorate-respirierenden Bakterien (PCRB), in welchen es entdeckt wurde, baut es das giftige Endprodukt der Atmungskette ab, und entflieht damit der Selbstvergiftung. Das Enzym und seine homologen Verwandten finden sich in verschiedenen bakteriellen und Archeen-Phyla und bioinformatische Untersuchungen suggerieren lateralen Gentransfer auch zwischen diesen Phyla. Trotzdem sind die meisten Stämme keine PCRB, darum ist die physiologische Aufgabe vieler Clds nicht offensichtlich und zeigen keine Chloritabbauaktivität.

Da die Verunreinigung durch Chlorit eher ein seit kurzem bestehendes Problem darstellt, das von industriellen Prozessen verursacht wird, ergibt sich die Frage nach der ursprünglichen evolutionären Funktion. Wasserverunreinigung durch Chlorit wurde zu einem ernsthaften Problem in den USA und Bioremediation durch Cld würde einen effizienten Weg darstellen um zu entgiften. Einige humanpathogene Krankheitserreger besitzen ein *cld*-Gen, darunter *Listeria monocytogenes*, dessen Cld-Genprodukt essenziell ist, was es zu einem möglichen potenziellen Angriffspunkt für Medikamente macht.

Basierend auf der Sequenz wurde versucht, die Cld-Aktivität vorherzusagen und einige Residues wurden vorgeschlagen als Signaturresidues für aktive Clds.

Ein Teil dieser Arbeit handelt von Mutationsstudien dieser Residues anhand der aktiven Cld von *Nitrospira defluvii* (kein PCRB) und den Effekt der Mutationen auf die enzymatischen Parameter.

Der zweite Teil befasst sich mit der Suche nach einer Funktion der Cld von *Listeria monocytogenes* (LmCld). Vorausgehende Untersuchungen zeigten keinen Beweis für die Anwesenheit von Häm-Bindung noch für Cld-Aktivität, darum lag der Hauptfokus darauf, einen Kofaktor zu finden, der eventuell eine andere Funktion vermitteln kann.

Im dritten Teil wird die Arbeit an der Cld von *Sulfolobus solfataricus* beschrieben, ein acidothermophiles Archaeon, dem der Schlüsselresidue für Cld-Aktivität zwar fehlt, aber die prosthetische Gruppe Häm bindet.

3. Introduction:

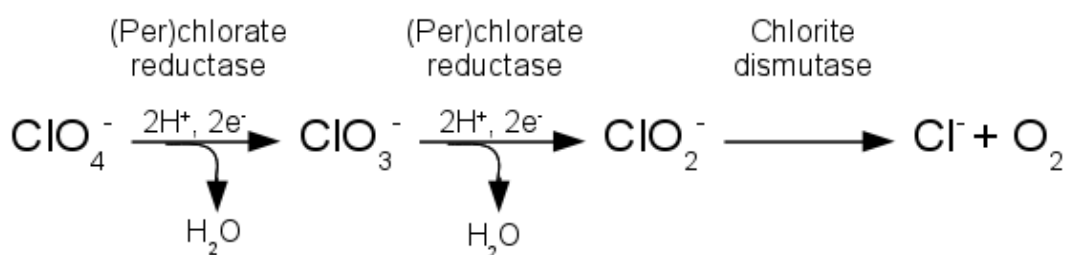
3.1. Oxochlorates

Most perchlorate found on earth is man-made, so the period of time microorganisms were exposed to perchlorate is very short. There is one natural source in Chile with up to 0.3‰ (w/w) perchlorate (Coates, 2004; Kengen and J., 1999). For industrial purposes perchlorate is produced by electrolysis of other oxochlorates and due to its strong oxidative nature is used as a bleaching reagent, anti-microbial agent and as an additive in rocket fuels (Urbansky, 1998; Urbansky, 2002).

The stability chlorine oxoacids in environmental conditions pronounces the need for proper degradation considering their threat to not only human health. Physical and chemical methods to do so proved to be difficult or failed (Coates, 2004) so bioremediation by PCRBs (perchlorate reducing bacteria) is one way to circumvent these obstacles (Wu, 2008).

For complete reduction of perchlorate to chloride microorganisms need two enzymes (see Figure 1). The first two steps of perchlorate reduction are catalyzed by perchlorate reductase (PerR), producing chlorite which is further reduced by the unique enzyme chlorite dismutase (Ueno, 2000). This enzyme is essential for PCRBs to circumvent the toxicity of chlorite. PerRs are homologous to nitrate reductases and Kengen et. al. (Kengen and J., 1999) suggest they evolved from them. Other sources speculate they evolved from DMSO (dimethylsulfoxide) reductase by gene duplication (Goblirsch et al., 2011). PerRs are promiscuous enzymes with the ability to reduce nitrate, iodate and bromate besides (per)chlorate. Some PCRBs show ability of nitrate respiration, too. (Coates, 2004).

Figure 1: Perchlorate reduction pathway (with kind permission of Kira Gysel, Diploma Thesis)



3.2. Chlorite Dismutase

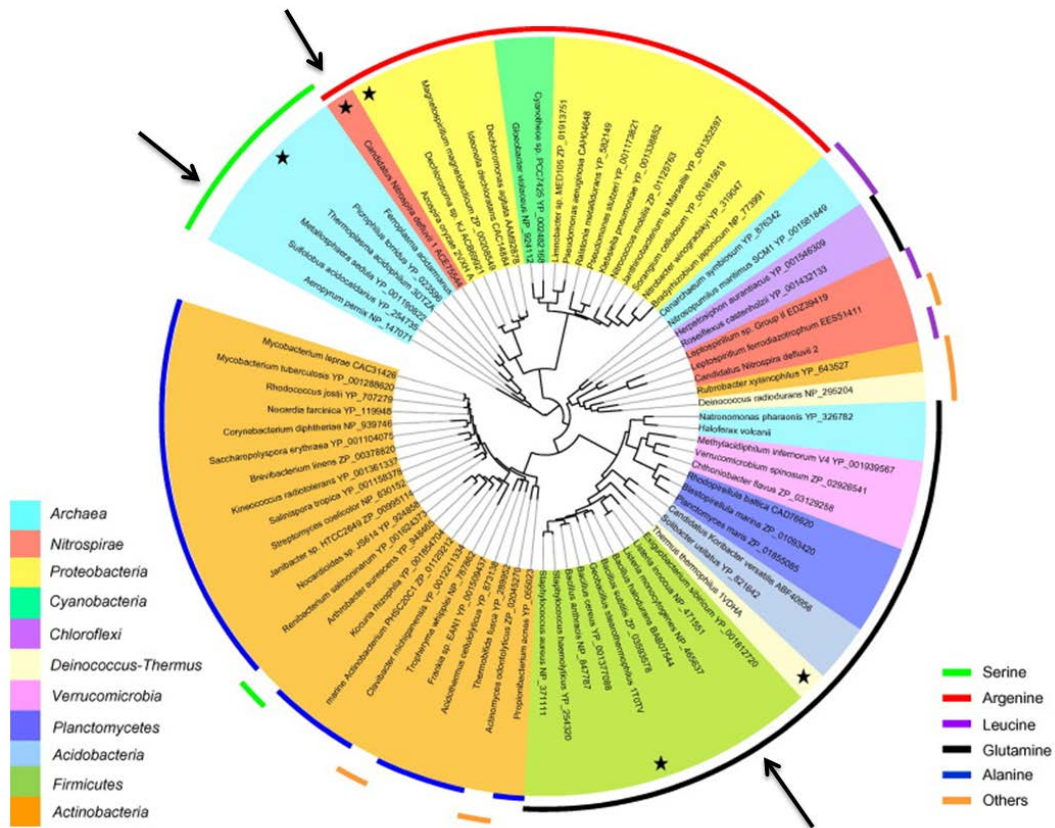
The reaction catalyzed by Cld is actually no dismutation but an intramolecular redox reaction. The correct name should be *chloride:oxygen oxidoreductase* or *chlorite O₂-lyase* (Hagedoorn, 2002). Still the name chlorite dismutase is mostly used in literature so it will be used throughout this thesis. Chlorite dismutase does not share any sequence similarities or obvious relationships with other well-characterized protein families. Compared to PerR or nitrate reductase substrate specificity Cld appears to be non-promiscuous (Brandon R. Goblirsch, 2010).

First discovered was Cld in PCRBs where the enzyme plays an essential role in the perchlorate reduction pathway (Bender et al., 2002). Yet environmental genomic approaches revealed many homologues in non-PCRBs, found in both bacterial and archaeal phylae (Maixner et al., 2008) and make up their own chlorite dismutase superfamily (Goblirsch et al., 2011).

Cld-activity was confirmed for a small fraction of this protein family, the validated Clds (termed active or canonical Clds in this thesis), but the function of the rest is still unknown (termed Cld-like proteins (Maixner et al., 2008)). Most likely the ability to degrade chlorite was only recently acquired by this protein family, whose members previously had a different purpose. Two factors indicate this: perchlorate is a recent anthropogenic pollutant (only a small number of microorganisms are specialized in perchlorate-respiration and experience selective pressure to decompose chlorite) and secondly in PCRBs the *cld*-gene is localized in the PerR operon, which it entered by horizontal gene transfer (Coates, 2004).

To map the various Clds and Cld-like proteins in a phylogenetic context several signature residues were suggested (Goblirsch et al., 2011; Kostan et al., 2010; Maixner et al., 2008; Mlynek et al., 2011). Structural and functional investigations show the importance of an arginine in the distal pocket of the heme (Arg173 in NdCld) and mutation studies underline its role in catalysis (Kostan et al., 2010). Moreover, they show that due to the conserved fold, the arginine and the corresponding residues are actually found at the same positions in the active site. This arginine and its corresponding residues are used to group Clds in a phylogeny tree (Figure 2, adapted from Kostan et al. (Kostan et al., 2010)). The only validated Clds are found within one branch, i. e. the one whose members all contain an arginine at this site.

Figure 2: Phylogeny tree of the chlorite dismutase family; asterisks mark the structurally characterized proteins, arrows indicate the representative proteins used in this thesis (adapted from (Kostan et al., 2010))



Based on these phylogenetic analyses Mlynek et. al. (Mlynek et al., 2011) proposed a classification of validated Clds into two lineages, one is comprised of the canonical Clds from PCRBs – Cld from *Nitrospira defluvii* (NdCld) being the only non-proteobacterial member – and the second lineage containing Cld from *Nitrobacter winogradskyi* (NwCld) and related proteins.

Apart from the validated and proposed active Clds there is a big cluster of related proteins with a glutamine at the position of the arginine. This “glutamine-cluster” contains many diverse bacterial species and also archaea. Also, there are some human pathogens found within, e. g. *Listeria monocytogenes* or *Staphylococcus aureus*.

Knock-out of the *cld*-gene in *Listeria monocytogenes* leaves the organism not viable (Füreder, 2009). Apart from that, neither Cld-activity nor electron density

for heme in X-ray crystallography experiments could be observed (Mlynek, 2010). Since *Listeria* as a facultative intracellular human pathogen is the cause of Listeriosis, this essential gene-product presents a potential drug target.

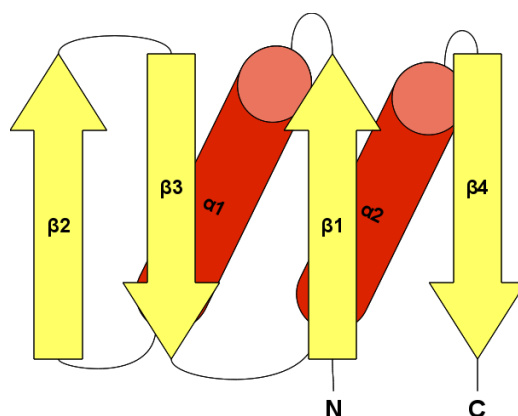
Another big cluster with alanine instead of the arginine includes Actinobacteria with e. g. *Mycobacterium leprae* and *Mycobacterium tuberculosis* being the most interesting ones, due to their human pathogenicity. Another branch is made of only archaeal species where the arginine is replaced by a serine.

Clds and Cld-like proteins are distributed over a many bacterial and archaeal phyla and share a common, ancient fold and sequence similarities. Validated Clds and proposed active Clds make up only a very small fraction of this protein family and the function of the rest remains unknown.

3.3. Structure of Chlorite Dismutases

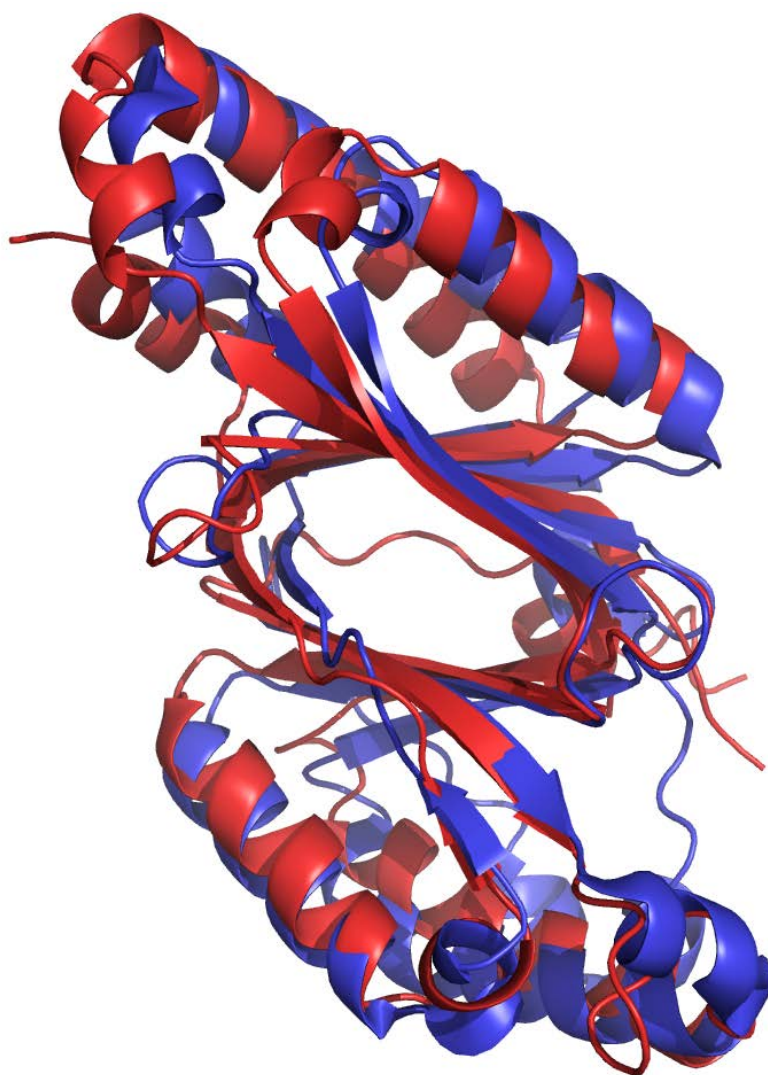
Crystal structures show a common and characteristic fold of all Clds and Cld-like proteins. Typically they are arranged as homo-oligomers (mostly homo-pentamers, but also homo-hexamers) where the oligomerisation state appears to have no effect on the catalytic efficiency (Hofbauer et al., 2012; Mlynek et al., 2011). Each subunit is made of two ferredoxin-like domains. The ferredoxin fold contains both α helices and β sheets, with the secondary structure motif β - α - β - β - α - β . The β strands form an antiparallel β sheet with the α helices packed against one side (Figure 3).

Figure 3: Topology diagram of a ferredoxin-like fold (Gysel, 2011)(with kind permission by Kira Gysel)



Clds consist of two structurally similar domains. The C-terminal ferredoxin-like domain coordinates the heme b *via* a conserved histidine residue on the proximal side of heme. Heme binding and the heme cavity structure is crucial for catalysis. The fold of these subunits is highly conserved, with a root mean square deviation of 1.72 Å between one subunit of an active Cld and a Cld-like protein over 180 Cα atoms (21).

Figure 4: Superposition of chain A of NdCld (3NN1, red) with LmCld (Cld-like protein, blue); r.m.s.d. of backbone atoms = 6.977 Å (667 to 667 atoms)



An exception to the structure described here is the already mentioned Cld from *Nitrobacter winogradskyi* (Mlynek et al., 2011). In contrast to the others, this enzyme is one third smaller in the primary sequence and lacks the α -helices of the N-terminal domain. The N-terminal part was probably lost during evolution (Mlynek et al., 2011). The C-terminal ferredoxin-like domain has an active site which is still very similar to other active members of the family. The reduced sequence does not let the subunits form homo-pentamers, NwCld forms homo-dimers with still high Cld-activity.

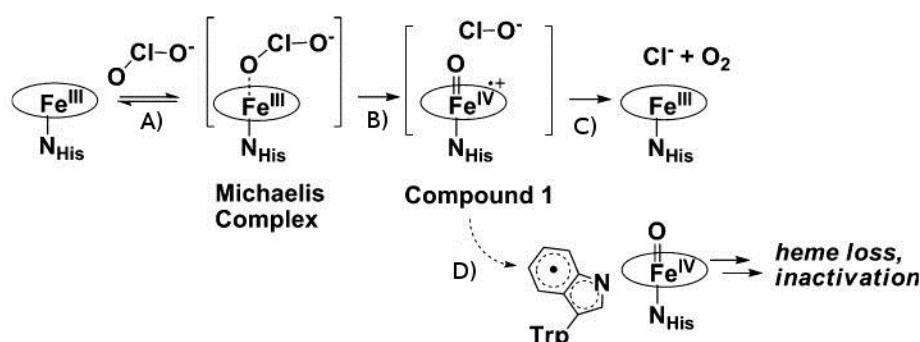
Cld-like proteins that contain no heme or show no Cld-activity have also been structurally analyzed, mostly of the lineage where glutamine replaces the arginine signature residue. The Cld structure of the thermophile bacterium *Thermus thermophilus* (TtCld) does not show heme, yet *in vitro* reconstitution with heme was partially successful (60% of subunits loaded with heme) which resulted in weak Cld-activity (Ebihara et al., 2005). On the other hand, *in vitro* binding of heme to recombinant LmCld was not observed (Mlynek, 2010). The option that in *Listeria monocytogenes* unidentified factors exist, that could mediate the uptake was tested in this thesis. A representative of the archaeal serine lineage, Cld of *Thermoplasma acidophilum*, was structurally analyzed by a structural genomics consortium and has no heme in the active site. The representative of this branch studied in this thesis from *Sulfolobus solfataricus* (SsCld) was shown to bind heme (see Section 6.9).

3.4. Reaction Mechanism

The most remarkable aspect of the reaction catalyzed by active Clds is the de novo formation of molecular oxygen. Only two other enzymes are known to be able to perform this kind of reaction as their primary function, namely water-plastoquinone oxidoreductase of photosystem II and a still uncharacterized enzyme from an anaerobic methane-oxidizer (Ettwig et al., 2010; Renger and Renger, 2008).

The mechanism of chlorite decomposition was proposed to be similar to the mechanism of heme peroxidases and catalases (Lee, 2008) *via* the intermediate Compound I state (see Figure 5), which was further modified by Kostan et al., Mlynek et al. and Goblirsch et al. (Goblirsch et al., 2011; Kostan et al., 2010; Mlynek et al., 2011).

Figure 5: Reaction mechanism of Cld; starting with ferric pentacoordinated iron; A) reversible collision to form the Michaelis Complex; B) Heterolytic cleavage of the Cl-O bond to form Compound I with Fe(IV); C) Nucleophilic attack of the intermediate hypochlorite and release of the products and recycled Fe(III); D) off-pathway generation of a tryptophan radical and enzyme inactivation; figure adapted from Goblirsch et al. (Goblirsch et al., 2011)



An alternative pathway including a homolytic cleavage of the Cl-O bond and formation of Compound II and radical hypochlorite has been proposed (Coates, 2004). Yet recent findings hint at the mechanism with the intermediate Compound I (Stefan Hofbauer, personal correspondence).

3.5. Catalytically Important Residues

The key residue arginine in active Clds (R173 in NdCld) plays an important role in substrate binding and stabilization of reaction intermediates. Apart from that, its positive charge is thought to position the substrate for proper catalysis (Mlynek et al., 2011). The conserved proximal histidine residue (H160 in NdCld), besides coordinating the prosthetic group, forms a H-bond to a conserved glutamate (E210 in NdCld). This interaction emphasizes the imidazolate character of the histidine, which in turn supports the ferric state of the heme iron. A tryptophan (W146 in NdCld) is thought to act as the electron donor and is also found in all Clds close to the propionate group of heme. Other conserved residues provide a proper environment for heme-binding, and have therefore been suggested to serve as signature residues for active Clds (I137 and L168 in NdCld) (Kostan et al., 2010).

3.6. Sources of Cld for this thesis

The sources of Clds used here exhibit several interesting aspects. They are all non-PCRBs with *Nitrospira defluvii* being the only organism with an active Cld. Their natural habitats and function within their environments make them interesting targets for intensive studying.

3.6.1. *Nitrospira defluvii*

Nitrospira defluvii are nitrite oxidizing bacteria, their genome was deciphered by environmental genomics from an activated sludge enrichment culture (Lucker et al., 2010). They are not close relatives to other nitrifiers and have probably evolved from microaerophilic or anaerobic progenitors. A periplasmic location signal peptide that precedes their *cld*-gene was removed these studies here as in (Kostan et al., 2010).

3.6.2. *Listeria monocytogenes*

Listeria monocytogenes is a gram-positive firmicute and the only human pathogen of the genus *Listeria*. *Listeria monocytogenes* as a facultative intracellular bacterium is the cause of listeriosis which still causes death in 20 – 30% of infected humans. The gene-product of their *cld*-gene is essential (Füreder, 2009) and might be targeted for medical treatment of listeriosis.

3.6.3. *Sulfolobus solfataricus*

Sulfolobus solfataricus belongs to the phylum of crenarcheota and is a thermoacidophile archaeon. It was first isolated from hot volcanic springs and its optimal growth conditions are at 80°C (60 – 92°C) and pH 2 – 4 (Zaparty et al., 2010). Its Cld is probably cytosolic and represents an interesting target for biochemical characterization since there are genetic tools like RNAi available for in situ functional analyses (Christa Schleper, personal correspondence).

4. Aim of this Thesis

The aim of this thesis was to gain deeper insight into the protein family of chlorite dismutases, its original and today's function. This can be divided into three parts, each dealing with a representative of different phyla.

One part continues the work on an active Cld, comprised of studies on NdCld (Cld from *Nitrospira defluvii*). The main goal was to gain deeper understanding of the Cld-reaction by mutating potentially relevant residues and analyzing their structural and enzymatic properties.

The second part aimed at finding a function for LmCld, which has been shown to be essential for the human pathogen *Listeria monocytogenes*. The starting point was the finding that recombinant LmCld, despite the presence of the heme-coordinating histidine, does not bind heme which is necessary for efficient catalysis of chlorite degradation. We aimed to assess the presence or absence of heme in LmCld from natural source and/or identify another cofactor and subsequently look for the function based on our findings.

The last part is centered on the archaeal lineage of Clds with the representative SsCld (Cld from *Sulfolobus solfataricus*). Proteins of this lineage contain a serine residue at the position of arginine in active Clds and have diverged from bacterial Clds early in evolution, most likely they perform reactions different from chlorite degradation. The goal was to establish recombinant overexpression and purification protocols to further investigate its enzymatic activity and biochemical, structural and biophysical properties.

5. Materials and methods

5.1. Media, Buffers and other Stock Solutions

Table 1: Antibiotics (purchased from Sigma Aldrich) were filtered (0,45 µm) and stored at -20°C

1000x Ampicillin/Carbencillin	100 mg/mL in H ₂ O
2000x Kanamycin	100 mg/mL in H ₂ O
1000x Chloramphenicol	34 mg/mL in ethanol

Table 2: Media, buffers and stock solutions

LB-Medium	10 g Tryptone, 5 g yeast extract, 10 g NaCl, adjusted to pH 7.0 with NaOH (ready-made, Sigma, 30 g for 1000 mL H ₂ O); autoclaved
LB-Agar	15 g agar in 1 L LB-medium
TBS	50 mM Tris (pH adjusted to according value with HCl), 150 mM NaCl
0,5M EDTA	EDTA solubilized with solid NaOH to final pH 8
50x TAE	2 M TrisHCl pH 8, 1 M acetic acid, 50 mM EDTA
TE	10 mM TrisHCl, 1 mM EDTA
10xSDS running buffer	0.25 M Tris-HCl pH 8.3, 2 M glycine, 1% (w/v) SDS
2x SDS loading	0.125 M TrisHCl pH 6.8, 6 M Urea, 2% SDS, 30% glycerol, 1 M β-mercaptoethanol, 0.1% Bromphenol blue
TBE	0.05 M Tris; 0,06 M boric acid; 0,001 M EDTA
2x heme-staining loading buffer	0.125 M TrisHCl pH 6.8, 6 M Urea, 4% SDS, 20% glycerol, 0.1% Bromphenol blue
Staining Solution	250 mL ethanol, 80 mL acetic acid, 2.5 g Coomassie brilliant blue, filled to 1000 mL with H ₂ O.
Heme	200 mg Hemin (Fluka) dissolved in 1.6 mL 0.5 M NaOH, filled to 40 mL with H ₂ O
IPTG	0.5 M IPTG in H ₂ O, sterile filtered (0.45 µm), stored at -20°C

5.2. Storage

Proteins were stored at 4°C for short term storage. For long term storage proteins were aliquoted to 100 µL, flash frozen in liquid Nitrogen and stored at -80°C.

DNA was stored in TE at -20°C.

Bacteria from 50 mL O/N culture were dissolved in 10 mL sterile filtered 15% glycerol, flash frozen and stored at -80°C.

Buffers and stock solution were stored at room temperature unless stated otherwise.

5.3. Cloning and Expression

Proteins were expressed in *E. coli* lab strains (Tuner (DE3), BL21 (DE3) or Rosetta2). For plasmid maintenance and mini-preps DH5α was used.

5.4. Expression vectors

The expression vectors all carry a copy of the *lacI* gene for the lac-repressor and thus are all inducible by addition of lactose or the artificial inducer Isopropyl-beta-D-thiogalactopyranoside (IPTG). The vectors include pETM11 with a TEV-cleavable 6x his-tag, pETM30 with TEV-cleavable 6x-his-GST-tag and a modified pET21(+) with a TEV-cleavable strep-tag II.

5.5. Constructs

All the constructs used during the work on this thesis are found in table 8. Most of the NdCld mutants were produced and purified together with Kira Gysel, who presented a more detailed analysis on the effects of mutated signature residues in her diploma thesis (Gysel, 2011).

5.6. Cloning

Site directed mutagenesis was used to create single or double mutants of the NdCld gene, for changing vectors conventional restriction enzymes were used. Restriction enzymes and respective buffers purchased from Fermentas. DNA concentration was determined spectroscopically with NanoDrop 2000c (ThermoFischer Scientific).

All oligonucleotides were ordered at Sigma-Aldrich on a synthesis scale of 0.2 μ mol, purified by desalting. The dry oligonucleotides were dissolved in 1x TE in an appropriate volume to reach a concentration of 100 μ M.

5.7. Site directed mutagenesis

To introduce point mutations of key residues in NdCld PCR (polymerase chain reaction) was used. For this purpose forward and reverse primers were designed, that carried the changed codon, where the reverse primer being the reverse complement of the forward primer. For double mutants the vector containing the single mutant gene was used as a template whereas for single mutants was the wild type vector.

PCR-protocol includes the 2x PhusionFlash MasterMix (Finnzymes), able to process 4 kb/min. PCR itself was carried out in an Eppendorf Mastercycler gradient PCR machine. To eliminate template DNA the PCR solutions were treated with Dpn1 (Fermentas) at 37°C for 1 h.

Table 3: List of primers for the constructs used or created during this thesis together with Kira Gysel (other NdCld mutation primers can be found in Kira Gysel's Diploma Thesis (Gysel, 2011)); changed codons marked red in fwd primers

Name	Primer sequence	T _M [°C]
W145V fwd	5'-GAAGGACGCGGAA GTG TGGGCACTGGACCAGG-3'	66
W145V rev	5'-CCTGGTCCAGTGCCCACACTTCCGCGTCCTTC-3'	66
W145F fwd	5'-TCCCTATCAAGAAGGACGCGGAA TTT TGGGCACTG-3'	62
W145F rev	5'-CAGTGCCCAAAATCCGCGTCCTTCTTGATAGGGA-3'	67
W146Y fwd	5'-GAAGGACGCGGAATGG TAC GCACTGGACCAGG-3'	64
W146Y rev	5'-CCTGGTCCAGTGCGTACCATTCCGCGTCCTTC-3'	64
W145V W146Y fwd	5'-GAAGGACGCGGAA GTG GCACTGGACCAGG-3'	63
W145V W146Y rev	5'-CCTGGTCCAGTGCGTACCATTCCGCGTCCTTC-3'	64
R173Q fwd	5'-CTGAAGACGGTGAAAC CAAA AACTGTATCATTTCG-3'	56
R173Q rev	5'-CGAATGATACAGTTTTTGTTCACCGTCTTCAG-3'	56
NwCld fwd	5'-GCTGAGCCATGGGGACGTTACAGTCTTCACC-3'	63
NwCld rev	5'-AGTTTCCTCGAGTCATATCGCGCGCCAATCGAAT-3'	63
LmCld fwd	5'-GCTGAGCCATGGGGATGAGCGATTACGACATCCC-3'	64
LmCld rev	5'-CCCCTCCTCGAGCTAAATAGTAAATAATTTAGAAAGTTG-3'	57
NdCld fwd	5'-GGAGATATACCCATGGCCGATC-3'	55
NdCld rev	5'-TTCGGATCCTACTGTGCGAACT-3'	55

5.8. Polymerase Chain Reaction

Table 4: PCR composition

Forward primer	0.2 µM	1 µl of 10 µM
Reverse primer	0.2 µM	1 µl of 10 µM
Template	15 ng	1 µl of 15 ng/µL
2x PhusionFlash	25 µL	
<u>MasterMix</u>		
add H2O to total of 50 µL		

Table 5: PCR settings

Process	Temperature [°C]	Time [sec]
Initial denaturation	95°C	300
Denaturation	95°C	30
Primer annealing	x°C	45
Extension	72°C	120
Cycles	30	
Final extension	72 °C	300
Cooling	4°C	hold

5.9. Transformation

100 µL of chemically competent cells (Hanahan, 1983) were put from -80°C to 4°C on ice, transformed with 5-20 ng DNA (or 6-10 µL of DpnI-treated PCR product after site-directed mutagenesis) and left on ice for 20 minutes. After a 45 - 60 sec heatshock (at 42°C), the cells were incubated again for 3 minutes on ice. Subsequently, 900 µL nonselective LB medium were added and the cells could recover at 37°C and 800 rpm for one hour in case of kanamycin and chloramphenicol resistance. Afterwards, the cells were plated onto a selective agar plate and grown in an incubator overnight at 37°C. For ampicillin resistance, cells were directly plated on selective agar.

5.10. Colony PCR

Before sequencing, newly transformed constructs were checked by colony PCR. Therefore single colonies were picked, dissolved in 5 µL sterile ddH₂O, of which 1µL was put on selective agar plates marked with a grid for later identification of the clones. Generic primers for the respective genes were used for amplification. The PCR products were analyzed on an 1 % agarose gel for the presence of a band at the corresponding size. Cells containing the desired insert from the plate were used for inoculation of a small-scale culture for mini-preps.

Table 6: Colony-PCR Composition

Component	Concentration	Volume	Stock
Cell suspension	-	4 µL	-
2x PhusionFlash	1x	12.5 µL	2x
MasterMix			
Primer fwd	0.8 µM	1 µL	10 µM
Primer rev	0.8 µM	1 µL	10 µM
add H ₂ O sterile to total of 25 µl			

Table 7: Colony-PCR settings

Cycle		
Process	Temperature [°C]	Time [sec]
Cell lysis	98°C	600
Initial denaturation	95°C	120
Denaturation	95°C	30
Annealing	x°C	54
Elongation	72°C	60
Cycles	30	
Final elongation	72°C	180
Cooling	4°C	Hold

5.11. Small Scale Plasmid Preparation (Mini-Prep)

For sequencing plasmids were extracted by the Plasmid Mini Kit from Fermentas. 5-10 mL of selective LB were inoculated with a single colony and incubated at 37°C, shaking over night. The dense cell cultures were harvested by centrifugation (15 minutes at 4000 rpm) and the plasmids purified according to the manufacturer's instructions (alkaline lysis method). The DNA was eluted from the spin columns with 30-50 µL TE buffer.

5.12. Subcloning

The expression vector was changed from pETM-11 (for Ndc1d, provided by Julius Kostan (Kostan et al., 2010)), from pET21b(+) (for LmCld, provided by Stephanie Füreder (Füreder, 2009)) or from pCR8-GW (for SsCld, provided by Andrea Manica) to a modified version of pET21(+) with an N-terminal Strep-Tag II, cleavable by TEV protease. This vector will be referred to as Strep-TEVpET21(+) throughout this thesis. The Cld insert was cut out with the restriction endonucleases NcoI (5'CCATGG-3') and XhoI (5'-CTCGAG-3'). The StrepTEVpET21(+) vector was cut with the same enzymes. The reaction mix consisted of 1 µg vector DNA, 5 µL 10x buffer R (Fermentas), 1 µL XhoI, 1 µL NcoI (both Fermentas, 10 U/µL). Sterile ddH₂O was added to a total volume of 50 µL and the mixture was incubated at 37°C for 1 h.

The digested DNA was purified on an 1 % (w/v) agarose gel containing cSYBR Safe DNA gel stain (Invitrogen, at a ratio of 1:10000) for UV visualization of the DNA. The bands were cut out from the gel, extracted with the GeneJET Gel extraction kit (Fermentas) and subsequently eluted from the spin column in 30 µL 1x TE.

The DNA yield was determined on the Nanodrop. The ligation reaction, which consisted of 1 µL 10x T4 ligation buffer, contained digested vector and insert at a molar ratio of 1:4 with approximately 20 ng of vector, 0.5 µL T4 ligase and sterile ddH₂O was added to a total volume of 10 µL. The ligation reaction was carried out at 16°C over night and the ligation product then transformed into *E. coli* DH5α.

Table 8: List of constructs

The following list contains all the constructs used and/or created during the thesis.

Construct	Insert	Vector	Tag
pJK23	NdCld	pETM-11	□x his
pJK29	LmCld□	□ETM-11	6x his
pJK30s	NdCld R173K	StrepTEVpET21	Strep tag II
pJK32s	NdCld R173L	StrepTEVpET21	Strep tag II
pJK53s	NdCld W146Y	StrepTEVpET21	Strep tag II
pJK54s	NdCld W145V	StrepTEVpET21	Strep tag II
pJK55s	NdCld W145V W146Y	StrepTEVpET21	Strep tag II
pKG1s	NdCld R173Q	StrepTEVpET21	Strep tag II
pKG3s	NdCld W146Y R173Q	StrepTEVpET21	Strep tag II
pKG4	LmCld	StrepTEVpET21	Strep tag II
pKG6	NdCld R173Q E210A	StrepTEVpET21	Strep tag II
pKG8	NdCld W145F	StrepTEVpET21	Strep tag II
pKG9	NdCld W145V R173E	StrepTEVpET21	Strep tag II
pKG10	SsCld	StrepTEVpET21	Strep tag II
pSF29	NwCld	pET21b(+)	6x his
pAH1	SsCld	pETM30	6x his-GST

For NdCld constructs (accession no. ACE75544), (Kostan et al., 2010) used a truncated version of the gene, lacking the predicted signal peptide for periplasmatic localisation (i. e. 26 N-terminal amino acids), since the full length construct was not functional.

Cld-like genes from *Listeria monocytogenes* (*Imo2113*, accession no. NC003210, provided by Stephanie Füreder), from *Sulfolobus solfataricus* (accession no. ACX92972.1) and from *Nitrobacter winogradskyi* (accession no. YP_319047) (Mlynek et al., 2011) were used full length. pETM-11 carries the resistance against kanamycin, pET21 the ampicillin resistance.

5.13. Protein Expression

Heterologous protein expression was carried out in *E. coli* lab strains. Pre-cultures were grown from a glycerol stock stored at -80°C by scratching the surface of a frozen stock with a pipette tip and were inoculated in 50 mL selective LB medium.

Protein expression at 18°C and 24°C was carried out in a coolable incubator shaker (Sartorius), at 37°C in a non-coolable incubator shaker (New Brunswick Scientific). The cells were harvested by centrifugation in 1 L centrifuge tubes using an SLC-4000 rotor at 4°C for 15 minutes at 5000 rpm in a coolable centrifuge (Sorvall Evolution RC Superspeed Centrifuge). The cell pellet was resuspended in 10 mL of the supernatant medium, transferred to a 50 mL Falcon tube and centrifuged again at 4000 rpm for 20 minutes at 4°C in an Eppendorf benchtop centrifuge.

Pellets were either further processed right away or otherwise flash frozen and stored at -80°C until usage.

5.13.1. NdCld: wild type and mutant expression

E. coli BL21 (DE3) Tuner cells carrying an expression vector for a NdCld mutant (see Table 8) were grown in 50 mL selective LB medium (pETM-11: Kanamycin; StrepTEVpET21: Ampicillin) at 37°C, shaking overnight. A 1/100 dilution was used for inoculation of selective LB and the cells were grown at 37°C to an OD₆₀₀ of 0.8. Then the temperature was reduced to 24°C, 50 mg hemin were added (1:1000, see 5.1) and the expression of NdCld induced with 0.5 mM IPTG. Cld was expressed 4 - 8 hours and the cells afterwards harvested by centrifugation, frozen in LN₂ and stored at -80°C.

5.13.2. NdCld: expression without heme („apoCld“)

E. coli BL21 (DE3) Tuner cells carrying the pJK23 plasmid (NdCld wild-type) were grown in 50 mL selective LB at 37°C over night. A 1/100 dilution was used for inoculation of selective LB and the cells were grown at 37°C to an OD₆₀₀ of 0.8. The protein expression was then induced with 0.5 mM IPTG and protein was expressed for 4 hours at 37°C. This yields the maximum amount of protein, while keeping the heme content as low as possible. The cells were harvested by centrifugation, the cell pellets flash-frozen in LN₂ and stored at -80°C until further use.

5.13.3. LmCld

E.coli BL21 (DE3) Tuner cells carrying either pJK29h or pKG4s were grown in 50 mL selective LB (kanamycin for pJK29h and ampicillin for pKG4, respectively) at 37°C shaking over night. A 1/100 dilution was used for inoculation of selective LB and the cells were grown at 37°C to an OD₆₀₀ of 0.8. Expression was induced by addition of IPTG to a final concentration of 0.5 mM and the cultures were cooled to 24°C, under agitation (160 rpm) for at least 4 h. Cells were then harvested by centrifugation, the pellets flash frozen and stored at -80°C until further use.

5.13.3. SsCld

E. coli Rosetta 2 pLysS cells transformed with pKG10 were grown in 50 mL LB supplemented with ampicillin and chloramphenicol over night at 37°C and this was used to inoculate selective LB, at 1/100 ratio. Cells grew at 37°C and 180 rpm to an OD₆₀₀ of 0.8 at which point they were induced to express by addition of IPTG to a final concentration of 0.25 mM and 50 mg heme per liter of culture and cooled down to 18°C, under agitation (160 rpm) for at least 8 h. Cells were then harvested by centrifugation, the pellets flash frozen and stored at -80°C until further use.

5.13.4. NwCld

E. coli BL21 (DE3) cells transformed with pKG10 were grown in 50 mL LB supplemented with ampicillin over night at 37°C and this was used to inoculate selective LB, at 1/100 ratio. Cells grew at 37°C and 180 rpm to an OD₆₀₀ of 0.8 at which point they were induced to express by addition of IPTG to a final concentration of 0.5 mM and 50 mg heme per liter of culture and cooled down to 18°C, under agitation (160 rpm) over night (ca. 16 h). Cells were then harvested by centrifugation, the pellets flash frozen and stored at -80°C until further use.

5.14. Protein Purification

Purification was done on ÄKTA PURIFIER systems (GE Healthcare) at 4°C. All columns were purchased from GE Healthcare.

Progress of the purification was monitored by measuring absorption at λ_1 = 280 nm, λ_2 = between 400 and 410 nm, which corresponds to the soret peak of bound heme and λ_3 = 360 nm, corresponding to the soret peak of free

heme. Extinction coefficients for A_{280} , according to Mlynec et al. (28) and Kostan et al. (21):

NdCld: $\epsilon = 37930 \text{ M}^{-1} \text{ cm}^{-1}$; $E 0.1\% (= 1 \text{ g/L}) = 1.382$

NwCld: $\epsilon = 40450 \text{ M}^{-1} \text{ cm}^{-1}$; $E 0.1\% (= 1 \text{ g/L}) = 1.984$

mutated NdClds, LmCld, SsCld: extinction coefficient taken from ProtParam (Gasteiger E, 2005)

LmCld: $\epsilon = 45505 \text{ M}^{-1} \text{ cm}^{-1}$; $E 0.1\% (= 1 \text{ g/L}) = 1,577$

SsCld: $\epsilon = 62340 \text{ M}^{-1} \text{ cm}^{-1}$; $E 0.1\% (= 1 \text{ g/L}) = 2.151$

Protein concentrations were always measured by UV absorption at 280 nm on the Thermo Scientific Nanodrop 2000c Spectrophotometer.

5.15. Purification conditions

5.15.1. Purification of NdCld wild type and mutants

Lysis buffer: 50 mM HEPES-NaOH pH 7.4, 5% (v/v) glycerol, 0.5% (v/v) Triton X-100

StrepTrap elution buffer: 20 mM HEPES-NaOH pH 7.4, 2% (v/v) glycerol, 2.5 mM Desthiobiotin

StrepTrap binding/dialysis/SEC buffer: 20 mM HEPES-NaOH pH 7.4, 2% (v/v) glycerol

5.15.2. Purification of Apo-NdCld

Lysis buffer: 50 mM HEPES-NaOH pH 7.4, 5% (v/v) glycerol, 0.5% (v/v) Triton X-100, 20 mM imidazole

HisTrap binding buffer: 20 mM HEPES-NaOH pH 7.4, 2% (v/v), 20 mM imidazole

HisTrap elution buffer: 20 mM HEPES-NaOH pH 7.4, 2% (v/v) glycerol, 500 mM imidazole

Dialysis/SEC buffer/AEX binding buffer: 20 mM HEPES-NaOH pH 7.4, 2% (v/v) glycerol

AEX elution buffer: 20 mM HEPES-NaOH pH 7.4, 2% (v/v) glycerol, 2 M NaCl

5.15.3. Purification of LmCld

Strep-tagged KG4s:

Lysis buffer: 50 mM TrisHCl pH 8.5, 150mM NaCl, 2% (v/v) glycerol

StrepTrap elution buffer: 50 mM TrisHCl pH 8.5, 150mM NaCl, 2% (v/v) glycerol, 2.5 mM Desthiobiotin

StrepTrap binding/Dialysis/SEC buffer: 20 mM TrisHCl pH 8.5, 150mM NaCl, 2% (v/v) glycerol

6x his-tagged JK29h:

Lysis buffer/HisTrap binding buffer: 50 mM TrisHCl pH 8.5, 150mM NaCl, 2% (v/v) glycerol, 20 mM imidazole

HisTrap elution buffer: 50 mM TrisHCl pH 8.5, 150mM NaCl, 2% (v/v) glycerol, 500 mM imidazole

Dialysis/SEC buffer: 50 mM TrisHCl pH 8.5, 150mM NaCl, 2% (v/v) glycerol

5.15.4. Purification of SsCld

Lysis buffer: 50 mM TrisHCl pH 9, 150mM NaCl, 2% (v/v) glycerol

StrepTrap elution buffer: 50 mM TrisHCl pH 9, 2% (v/v) glycerol, 2.5 mM Desthiobiotin

StrepTrap binding/Dialysis/SEC buffer: 20 mM TrisHCl pH p, 2% (v/v) glycerol

5.15.5. Purification of NwCld

Lysis buffer: 50 mM TrisHCl pH 8.5, 150mM NaCl, 2% (v/v) glycerol, 0.5% (v/v) Triton X-100, 20 mM imidazole

HisTrap binding buffer: 50 mM TrisHCl pH 8.5, 150mM NaCl, 2% (v/v) glycerol, 20 mM imidazole

HisTrap elution buffer: 50 mM TrisHCl pH 8.5, 150mM NaCl, 2% (v/v) glycerol, 500 mM imidazole

Dialysis/SEC buffer: 50 mM TrisHCl pH 8.5, 150mM NaCl, 2% (v/v) glycerol

Cell pellets were thawed and resuspended in 35 mL Lysis buffer per L culture. Cells were broken either by sonication (3 x 5 minutes, 3 cycles, 70% power) or on a french press and the Crude extract subsequently cleared by centrifugation (SS34 rotor) at 4°C, 38,000 g for 15 minutes.

5.16. Strep-Tactin Affinity

For the proteins that were expressed with an N-terminal Strep-Tag II, the clear supernatant was loaded on a clean StrepTrap HP column previously equilibrated with StrepTrap binding buffer, washed with 5 CV binding buffer and subsequently eluted with a step gradient of 2.5 mM Desthiobiotin in the Strep-Trap elution buffer. After analysis by SDS-PAGE, the fractions containing Cld were pooled together.

5.17. Ni-NTA Affinity

For constructs containing a 6x His tag, the clear supernatant was loaded on a clean HisTrap HP column previously equilibrated with HisTrap binding buffer, washed with 5 CV binding buffer and subsequently eluted with a linear gradient of HisTrap elution buffer. After analysis by SDS-PAGE, the fractions containing Cld were pooled together.

5.18. Further purification

After affinity purification the tag was cleaved off with TEV protease. The fractions containing the protein were pooled and transferred to a dialysis bag with a molecular weight cut-off of 12,000 - 14,000 Da, TEV protease added at a 1:30 - 1:50 mass ratio and dialyzed overnight at 4°C against 1 L of dialysis buffer with 1 mL mercaptoethanol. Uncleaved protein was then removed by another affinity purification step, where only the flow-through was collected. This step also gets rid of 6x his-tagged TEV in case of Ni-NTA affinity. Cleavage of the tag was monitored by SDS-PAGE. For heme-binding proteins, heme (freshly prepared see section 5.1) was added to the protein solution at a molar ratio of 2:1 heme:protein and left on 4°C for 30 – 60 min. Insoluble heme was then removed by spinning for 30 minutes at 18,000 rpm at 4°C.

The protein solutions were concentrated in an Amicon Ultra centrifugal filter unit (Milipore) with a molecular weight cut-off of 30,000 or 50,000 to a volume of about 5 mL (which also removes most of the remaining TEV protease in case of the Strep-Tactin based purification) and loaded on an equilibrated Superdex 200 16/60 size exclusion column.

Pure protein was further concentrated in an Amicon Ultra centrifugal filter unit to 5-30 mg/mL (depending on solubility), divided to 100 µL aliquots, flash-frozen in liquid nitrogen and stored at -80°C.

For production of apoNdCld an additional anion exchange step before SEC was included to get rid of partially loaded NdCld. Previous observations showed a different behaviour of loaded and unloaded NdCld on an anion exchange column (based on the differences between the ratios of A_{280}/A_{Soret}). The sample was loaded on a 6 mL ResourceQ AEX column equilibrated with SEC buffer. A washing step with 5% of AEX elution buffer (corresponds to 100 mM NaCl and approximately 11.5 mS/cm) to remove heme-loaded NdCld. A linear salt gradient over 15 CV to 20% AEX elution buffer (corresponding to 400 mM NaCl) let the desired fractions elute (usually at about 16 mS/cm), confirmed by spectrometrically determining the ratio A_{280}/A_{Soret} . NdCld was declared apoCld when A_{280}/A_{Soret} was about 1/10.

5.19. Immuno-precipitation

Binding buffer: TrisHCl pH 7.5, 150mM NaCl

Elution buffer: TrisHCl pH 7.5, 150mM NaCl, 3 M urea, 10 mM DTT

Immuno-precipitation of native LmCld was done by polyclonal rabbit anti-LmCld antibodies (kindly provided by Stephanie Füreder) and magnetic Protein A beads (GE Healthcare).

The *Listeria monocytogenes* lab strain LO28 was grown under anaerobic conditions, since it has been reported that under these conditions the expression of LmCld was slightly upregulated. Cell pellets were frozen and stored at -80°C and kindly provided by Thomas Decker.

Cells were resuspended in binding buffer with appropriate amounts of the protease inhibitor cocktail complete EDTA-free (Roche) (pellet from 1L culture in 20ml) and lysed by sonication (2 x 4 minutes, 3 cycles, 70% power). Cell debris was removed by centrifugation (SS34 rotor) at 4°C, 38,000 g for 15 minutes. This centrifugation step alone led to precipitation in the pull-down step so an additional ultra centrifugation step was applied (100 000 g at 4°C for 1 h).

Magnetic Protein A beads were prepared by equilibration with the binding buffer and subsequent addition of polyclonal anti-serum with the antibodies in excess to prevent binding of other immunoglobulins than immunoglobulin G. Protein A is a membrane bound protein produced by *Staphylococcus aureus* to prevent opsonization by the immune system due to its high affinity for the IgG-Fc domain thereby hindering interaction of the IgG epitopes with their para-

topes and the interaction of their Fc-region with other factors involved in the classical complement pathway.

After binding of IgG to the Protein A beads the beads were washed 3x by adding 500 μ L binding buffer and vortexing for 3 – 5 sec and removal of the buffer.

Protein A – IgG beads were then applied to the cleared lysate, to minimize un-specific binding in a ratio of 10 μ L beads in 8 mL of lysate. The pull-down step was performed on a spinning wheel at 4°C for 4 - 8 h.

The solution was removed and the beads washed 6x with binding buffer, including one wash step with increased NaCl concentration (500 mM instead of 150 mM) to improve purity. Each step consists of addition of 500 μ L buffer, gentle vortexing for 3 – 5 sec and removal of the buffer.

Beads with native LmCld bound were either stored in binding buffer at 4°C, cooked in SDS-sample buffer for conventional SDS PAGE, incubated in heme-staining sample buffer for 20 min at room temperature or the protein was eluted by addition of elution buffer. Depending on the next step in line the protein was concentrated when necessary.

The identity of the pulled down protein was verified by mass spectrometry (BSRC Mass Spectrometry and Proteomic Facility St. Andrews).

5.20. Heme staining

2x sample buffer: 0.125 M TrisHCl pH 6,8, 6 M urea, 4% SDS, 20% glycerol, bromphenol blue

Running buffer: 0.05 M Tris, 0.06 M boric acid, 0.001 M EDTA (TBE)

Staining solution: 200 mg o-dianisidine (=DMB, 3',3'-dimethoxybenzidine; Sigma-Aldrich) stirring in 180 mL H₂O; before staining addition of 20 mL of 0.5 M sodium citrate pH 4.4 and 0.4 mL of 30% H₂O₂

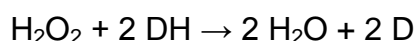
The heme staining protocol by Francis and Becker (Francis RT Jr, 1984) offers means to stain heme still bound to the electrophoretically separated protein. Here a modified version was used, since the elution from the Protein A beads needed harsher conditions. In these conditions a non-covalently bound heme dissociates and migrates at the dye front. The reported limit of detection of 40 pmol heme was confirmed here.

An equal amount of 2x sample buffer was added to the samples and incubated for 20 min at room temperature. Samples were applied to a normal 15% poly-

acrylamide gel, electrophoresis was performed at 4°C for 1.5 – 2 h with 15mA in the running buffer TBE.

Proteins and heme were fixed by treatment with 12.5% TCA for 30 min on a benchtop shaker and then washed with ddH₂O for 30 min followed by shaking in the staining solution for one hour.

The reaction occurring during staining relies on the intrinsic peroxidase activity of heme, o-dianisidine binds to heme and heme catalyses the transfer of two hydrogen atoms to H₂O₂, the net reaction being



where DH is the reduced version and D is the oxidized version of the donor.

The donor in this case is o-dianisidine and upon oxidation it changes its color to a brownish red when bound to protein and green when dissociated. This redox reaction is also the reason for the non-reducing conditions in the sample buffer.

This procedure stains both the dissociated heme from proteins to which it was not covalently bound and heme still attached to proteins. Due to the absence of SDS in the running buffer the migration of proteins is slower as compared to the migration in conventional SDS PAGE resulting in impaired separation between proteins present in the respective samples. Therefore a conventional SDS PAGE was always performed in parallel to check for impurities.

After heme staining the gels can optionally be stained by coomassie blue to optically analyze the protein migration. Note that o-dianisidine also has affinity for coomassie blue and will be stained as well.

5.21. Fluorescence based thermal shift assay

The assay relies on measuring fluorescence of the hydrophobic dye SYPRO orange (Invitrogen), which is quenched when surrounded by water molecules (Reinhard L, 2013). Upon heating on the real time PCR thermocycler (BioRad iQ5 Multicolor Real-Time PCR Detection System; 1°C per minute) the protein starts to unfold, thereby exposing hydrophobic patches that are then available for binding of the hydrophobic dye. Interaction between dye and hydrophobic parts of the protein diminishes the quenching effects of water. This way, the more protein is unfolded, the more fluorescent signal is measured and the temperature where half of the protein is unfolded is considered the melting temperature.

Three commercial screens were applied to recombinant LmCld with cleaved Strep-tag II, namely Additive Screen, Silver Bullets and Silver Bullets Bio (all Hampton Research).

4 mg of protein, 2 μ L SYPRO orange and SEC buffer to a total of 22.5 μ L were dispensed into a RT-PCR plate. 2.5 μ L of each condition of the different screens were dispensed by Phoenix liquid handling system (Art Robbins Instruments) and mixed three times. The plates were sealed and centrifuged before measurements.

The melting temperatures were compared and the compounds found to be increasing the T_M of the protein are shown in Figures 6 - 8 and Tables 10 - 12.

5.22. Crystallography

5.22.1. Robotics and Materials

Initial crystallization trials were done by sitting drop vapour diffusion in 96-well plates Phoenix liquid handling system (Art Robbins Instruments).

Optimization of crystallization conditions were done by using an Alchemist II liquid handling robot (Rigaku) for dispensing of non-commercial optimization screens in either 96-well plates and sitting drop vapour diffusion or in 24-well Linbro format hanging drop plates.

96-well sitting drop plates were inspected by a Minstrel DT imaging system (Rigaku) equipped with the Atlantis software for automatic imaging in combination with CrystalTrak software (Rigaku).

Plates used were 96-well IntelliPlates (Art Robbins instruments) with 3 slots for the drops and 24-well pregreased Linbro plates (Crystalgen) which were set up manually.

Crystals were stored in an temperature regulated room at either 22°C or 4°C.

5.22.2. Crystallization of LmCld

Pure recombinant LmCld from strep-affinity purification at 7.33 mg/mL showed positive hits in the SaltRX screen (Hampton) of which two conditions were used for optimization. These were chemically similar, i. e. the pH was slightly alkaline and the precipitating salts were both organic acids (tartrate and citrate,

respectively). According to the diffraction power of the crystals formed, the condition chosen for crystallization was derived from condition 87 of SaltRX (Hampton Research).

In this condition multiple nucleation was observed. To overcome this obstacle glycerol concentration was increased to 8% (v/v) in order to slow down the vapour diffusion kinetics.

For cryo protection the glycerol concentration was further elevated to 25% (v/v) by adding mother liquor with glycerol to the drops.

5.22.3. Crystallization of LmCld with additives

The optimized condition was then applied to LmCld together with selected additives (see section 6.1) in the same ratio as in the thermofluor studies. Protein and additives were mixed prior to crystallization and divided in two, one of which was centrifuged at 16,000 g, 4°C and both crystallized in parallel. Crystallization with additives was done in 24-well Linbro plates only. For final crystallization conditions see table of crystallization conditions (Table 9).

For cryo protection the glycerol concentration raised to 25% (v/v) by adding mother liquid with glycerol to the drops. Transfer to drops with higher concentrations was undesirable, since it might have caused the additives to be washed out.

5.22.4. Crystallization of NdCld W145F

In contrast to other constructs this mutant was crystallized still attached to the strep-tag, hence leaving out the TEV protease in the dialysis step (see section 5.18). The rationale behind this was the observation that degradation took place when treated with TEV whereas without TEV it did not. Initial attempts to crystallize this mutant in conditions similar to wild type and other NdCld mutants (high ammonium sulfate, citrate buffer pH 3.5 – 4.5; derived from condition 13 of JCSG+, Qiagen) gave crystals growing in only two dimensions, i. e. they were plate-shaped.

Screening for better conditions with commercial screens provided a few starting conditions, from those a condition similar to the previously mentioned conditions was selected (condition 15 from SaltRX, Hampton). There, the citric acid was used as precipitant instead of buffering agent together with ammonium, buffered by sodium acetate.

For cryo protection the crystal were soaked in increasing concentrations of ethylen glycol, since the crystals were impaired when using high glycerol concentrations. Stepwise increase of 5% (v/v) of ethylen glycol in mother liquid to a final concentration of 30% (v/v) left the crystals unharmed.

The structure of the W145F mutant was also solved in complex with the inhibitor cyanide, which binds to the heme iron. KCN was dissolved in SEC buffer (see section 5.15.1) and was added in 2-fold excess to the protein solution and incubated for 1 h at room temperature prior to crystallization.

Table 9: Crystallization conditions

Construct and additives	Condition	Drop [μ L]	Cryo protectant
LmCld	1 M Na K tartrate, 8% glycerol, 0.1 M TrisHCl pH 9	2:1 hanging	25% (v/v) glycerol
LmCld BaCl ₂ (AS1)	1.15 M Na K tartrate, 8% glycerol, 0.1 M TrisHCl pH 9	0.5 : 0.5 hanging	25% (v/v) glycerol
LmCld CdCl ₂ , CoCl ₂ , CuCl ₂ , NiCl ₂ (SB42)	1 M Na K tartrate, 8% glycerol, 0.1 M TrisHCl pH 9	1 : 0.5 hanging	25% (v/v) glycerol
LmCld YCl ₃ (AS9)	1.15 M Na K tartrate, 8% glycerol, 0.1 M TrisHCl pH 9	1 : 0.5 hanging	25% (v/v) glycerol
LmCld CdCl ₂ , CaCl ₂ , MgCl ₂ , MnCl ₂ , ZnCl ₂ (SBB46)	1 M Na K tartrate, 8% glycerol, 0.1 M TrisHCl pH 9	1 : 0.5 hanging	25% (v/v) glycerol
LmCld GdCl ₃ , SaCl ₃ , benzamidineCl, salicin (SB40)	1 M Na K tartrate, 8% glycerol, 0.1 M TrisHCl pH 9	1 : 0.5 hanging	25% (v/v) glycerol
LmCld FeCl ₃ (AS11)	1.2 M Na K tartrate, 8% glycerol, 0.1 M TrisHCl pH 9	1 : 0.5 hanging	25% (v/v) glycerol
LmCld protamine sulfate (SB52)	1.1 M Na K tartrate, 8% glycerol, 0.1 M TrisHCl pH 9	1 : 0.5 hanging	25% (v/v) glycerol
NdCld W145F	0.7 M Ammonium citrate dibasic, 0.1 M Na acetate pH 4.4	2:1, hanging	30% (v/v) ethylen glycol
NdCld W145F + cyanide	0.78 M Ammonium citrate dibasic, 0.1 M Na acetate pH 4.53	2:1, hanging	30% (v/v) ethylen glycol

In Brackets you find the screen and number of the respective conditions, with the abbreviations being AS: Additive Screen, Hampton; SB: Silver Bullets, Hampton; SBB: Silver Bullets Bio, Hampton

Additives were used as suggested by the manufacturer. LmCld was used at 7.4 mg/mL, NdCld W145F at 10 mg/mL

5.23. Structure Determination

5.23.1. Data Collection

Diffraction data were collected at synchrotron beamlines (ESRF ID 23-1, BESSY ID14-1). Integration and scaling was done with XDS and XSCALE (Kabsch, 2010).

5.23.2. Molecular Replacement

The phases for all data sets were derived from molecular replacement by the online server software BALBES (Long et al., 2008).

5.23.3. Refinement

Refinement of LmCld structures was carried out in Phenix Refine (Adams et al., 2010) and Coot (Emsley, 2010). Refinement of NdCld W145F was refined in Refmac5 (Collaborative Computational Project, 1994; Murshudov et al., 2011).

5.23.4. Localization of Anomalous Scatterers

Data collection was done at wavelengths close to the absorption edges of the respective metal ions from the additive screens (see section 6.1). mtz files of the solved structure of LmCld and the ones from data sets taken at appropriate wavelengths were combined in Cad (Collaborative Computational Project, 1994) of the CCP4 software suite. The combined mtz files were used to create an anomalous difference map carried out in FFT (Collaborative Computational Project, 1994) of the CCP4 software suite.

5.24. Steady-state Kinetics

The activity of NdCld mutants and SsCld was determined by measuring the oxygen created when the enzyme is processing its substrate, ClO₂ or H₂O₂ respectively. This was measured with a Clark-type electrode (Oxygraph System, Hansatech Instruments, Norfolk, UK) in a stirred water bath at a constant temperature between 30°C and 45°C. Buffers for measurements include 100 mM phosphate buffer, pH 7.0 for NdCld, 100 mM Sodium Acetate, pH 6.25 and 5.5, an 100 mM TrisHCl, pH 9 for SsCld. The electrode was equilibrated to 100% O₂ saturation by bubbling O₂ to a blank reaction mixture for 10 minutes

and with 0% O₂ by bubbling with N₂ for another 10 minutes, removing all the oxygen from the solution.

For activity measurements the substrate was injected to the cell in increasing concentrations of 25 - 1000 µM ClO₂ and 5 – 930 mM H₂O₂. The buffer-substrate solution (total volume of 1mL) was purged from all oxygen by bubbling the solution with N₂ until a stable baseline was reached. Subsequently the reaction was initiated by injecting 20 µL of a protein solution into the cell with a hamilton syringe to a final concentration of about 100 nM for NdCld and 500 nM for SsCld.

For calculations only the initial linear slope was used. Production of molecular oxygen (in [M O₂ s⁻¹]) was determined and plotted against chlorite concentrations and H₂O₂ concentration, respectively, in SigmaPlot (Systat Software Inc., v12). For fitting and calculation of the values of the kinetic constants of the enzyme the Michaelis-Menten formula was employed:

K_M , the Michaelis constant by the formula – $K_M = v_{max}/2$ [µM];

k_{cat} , the turnover number [s⁻¹] and

k_{cat}/K_M , the catalytic efficiency of the enzyme [M⁻¹ s⁻¹].

5.25. Static Light Scattering

SLS was employed to determine the molecular weight and the radius of gyration of purified proteins. In this case the goal was to determine the oligomeric state of the protein (Murphy, 1997).

The system consisted of a miniDawn Treos (Wyatt) light scattering detection system connected to a refractometer (RI-101, MD Scientific) and an HPLC (1260 Infinity HPLC, Agilent).

Separation of different oligomeric species was done on a Superdex 200 10/300 analytical SEC column which was equilibrated with SEC buffer until the baseline stabilized. NwCld was also dissolved in NdCld SEC buffer (buffer exchange with BioRad MicroSpin Column). Protein solutions were diluted to 2 mg/mL (with the exception NwCld was used as at 1 mg/mL) and 70 µL were used for each run. Protein elution was monitored by absorption at 280 nm and the correlating molecular mass determined by static light scattering.

5.26. UV-vis spectroscopy

Heme binding and content were monitored on a UV-vis spectrophotometer Hitachi U-3900 with quartz cuvettes of 10 mm pathlength.

6. Results

6.1. Thermal Shift Assay

Purified recombinant LmCld was used for thermal shift measurements in which the thermal stability of the protein was determined. Comparison of the melting temperature T_M of the protein in different solutions was conducted to identify potential specifically binding additives.

Since there is no known function for any Cld-like protein and LmCld appears to be essential for *Listeria monocytogenes* (Füreder, 2009), the question arises if there is another cofactor that aids in the proteins enzymatic activity. If a cofactor exists that specifically binds to LmCld, the assumption that specific binding would lead to stabilization was the basis for this shot-in-the-dark experiment.

Figure 6: Thermofluor of LmCld with Additive Screen

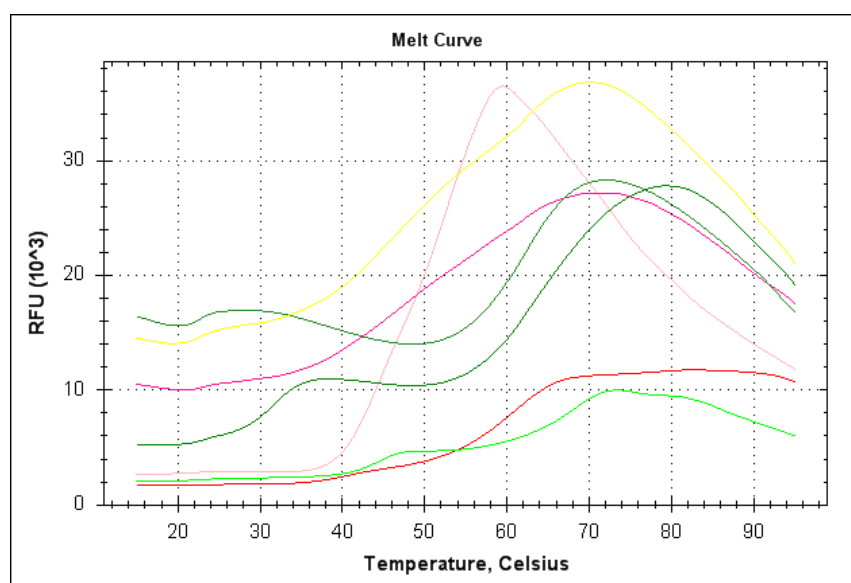
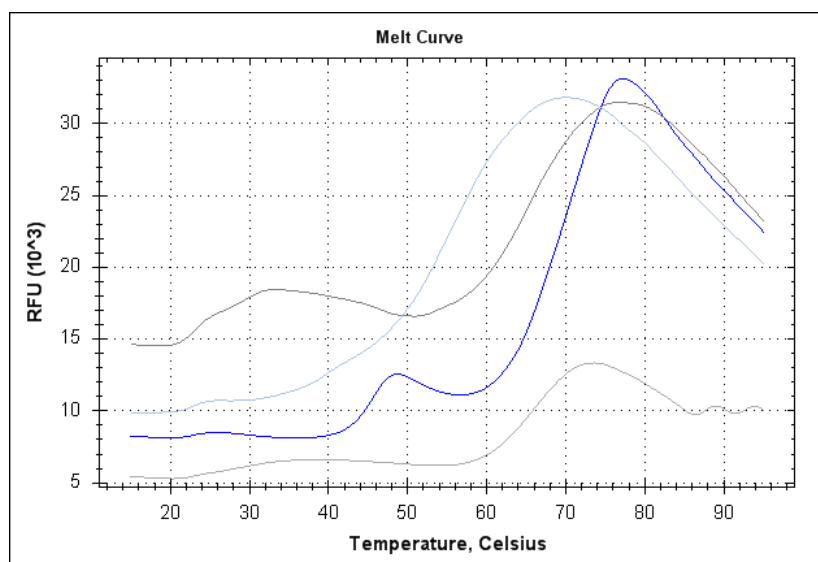


Table 10: Stabilizing conditions of Additive Screen

Reagent Nr.	Formula	T _M
1	BaCl ₂	68°C
2	CdCl ₂	62.5°C
9	YCl ₃	62.5°C
10	ZiCl ₂	62.5°C
12	NiCl ₂	61°C
14	Pr(III) acetate	62.5°C
Control	NaCl	53°C

Figure 7: Thermofluor of LmCld with Silver Bullets**Table 11:** Stabilizing conditions of Silver Bullets

Reagent Nr.	Formula	T _M
40	GdCl ₃ , SaCl ₃ , benzamidineCl, salicin	55°C
41	CaCl ₂ , MgCl ₂ , MnCl ₂ , ZnCl ₂	65°C
42	CdCl ₂ , CoCl ₂ , CuCl ₂ , NiCl ₂	65.5°C
52	Protamine sulfate	70.5°C

Figure 8: Thermofluor of LmCld with Silver Bullets Bio

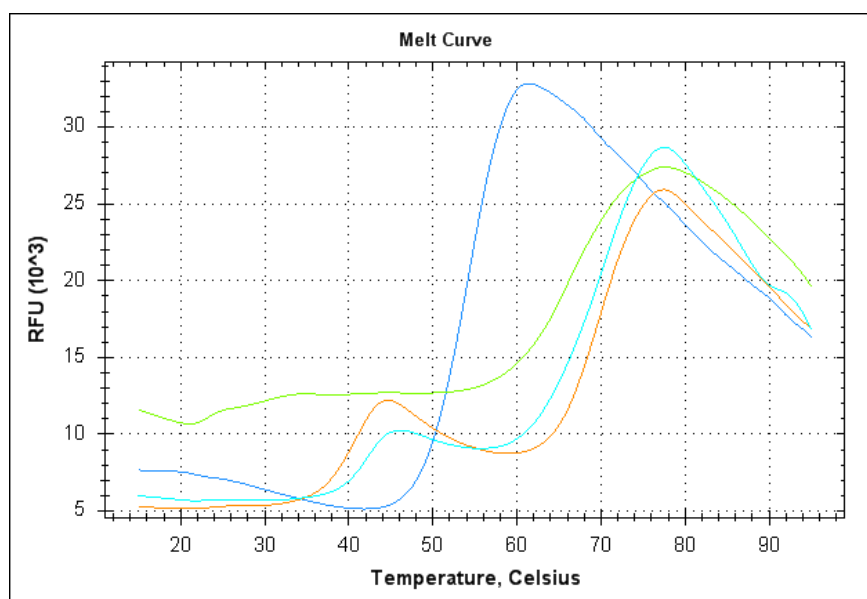


Table 12: Stabilizing conditions of Silver Bullets Bio

Reagent Nr.	Formula	T _M
11	Protamine sulfate, g-Strophanthin, Benzamidine hydrochloride, D-Fructose 1,6-diphosphate trisodium salt octahydrate, Oxamic acid	55°C
20	Protamine sulfate, Ellipticine, D-(+)-Trehalose dihydrate, 6-Phosphogluconic acid trisodium salt, D-(+)-Glucose	65°C
46	CaCl ₂ , CdCl ₂ , MgCl ₂ , MnCl ₂ , ZnCl ₂	65.5°C
76	Pyridoxal hydrochloride, Nicotinamide, Batyl Alcohol, Glutaric acid, N-Acetyl-L-glutamic acid	70.5°C

Both the Silver Bullets and the Silver Bullets Bio are designed in a redundant way, meaning that a specific compound is found in more than one condition. This makes it possible to identify the stabilizing compound in the mixture. For example mixtures containing the arginine-rich polypeptide protamine showed stabilizing effects to different degrees. The highest T_M was measured in the Silver Bullets condition 52, where protamine sulfate is the only compound.

Condition 76 of Silver Bullets Bio gave a high T_M too, but none of the other conditions containing one of those compounds showed improvement in the protein's stability. This mixture was therefore not selected for crystallization.

Several conditions containing one kind of salt from Additive Screen could be found in mixtures in the Silver Bullets screens. Due to low availability of protein the mixtures were selected for co-crystallization.

The main question arising from this experiment was, if the stabilizing compounds bind specifically or have unspecific stabilizing effects. The attempt to answer this was done by co-crystallizing selected conditions with LmCld (see section 6.1).

FeCl_3 of condition 11 from Additive Screen did not give an interpretable curve in the thermofluor measurements. Nevertheless it was used for co-crystallization because of the results from ICP-MS (see Section 6.5.3).

6.2. Structure of recombinant LmCld

Recombinant LmCld was crystallized before by Georg Mlynek (Mlynek, 2010), showing high similarity to the active Cld from *Nitrospira defluvii*. Both are pentameric proteins with the same fold, i. e. two ferredoxin-like domains arranged in the same way (see Figure 12). In contrast to NdCld, LmCld does not show any electron density in the active site cavity of the C-terminal ferredoxin domain. Although the heme-coordinating proximal histidine is present, some other residues appear in positions that might clash with heme when bound (see figure 9), assuming no structural rearrangements. Moreover, the α -helix containing the conserved histidine is slightly more tilted towards the cavity, leaving less room for potential heme-binding.

By steady-state kinetic measurements of mutants, the key residue for active Clds was shown to be Arg173 in NdCld (Kostan et al., 2010). All validated Clds contain arginine at the corresponding position. The arginine alone is not enough for Cld-activity, the presence of heme is critical for the protein to exert catalysis. In the case of LmCld the residues comprising the potential heme environment do not favour its binding (figure 9 and 10) and therefore it cannot be catalytically active.

Figure 9: Residues of LmCld clashing with heme. A superposition of LmCld (green) and NdCld (magenta); Coordinating histidine, key residue arginine and heme of NdCld and the clashing residues Y147, G178, I215 and M219 of LmCld are shown

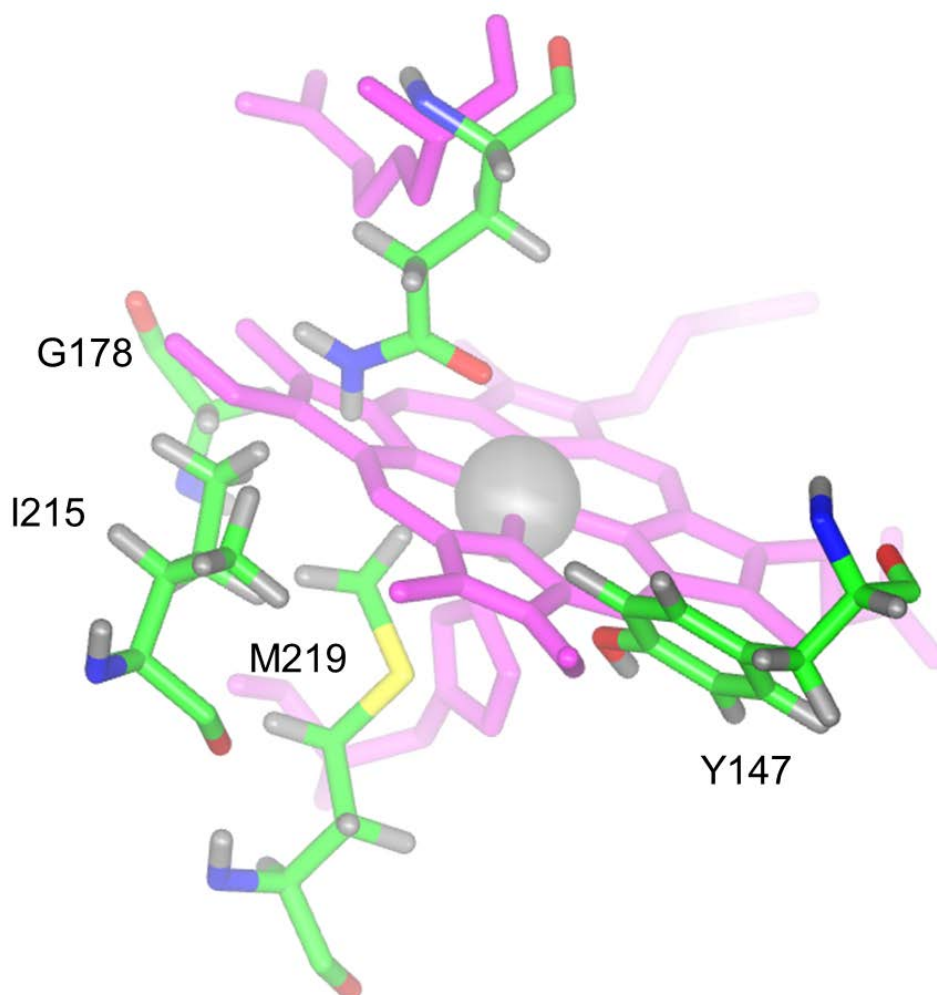
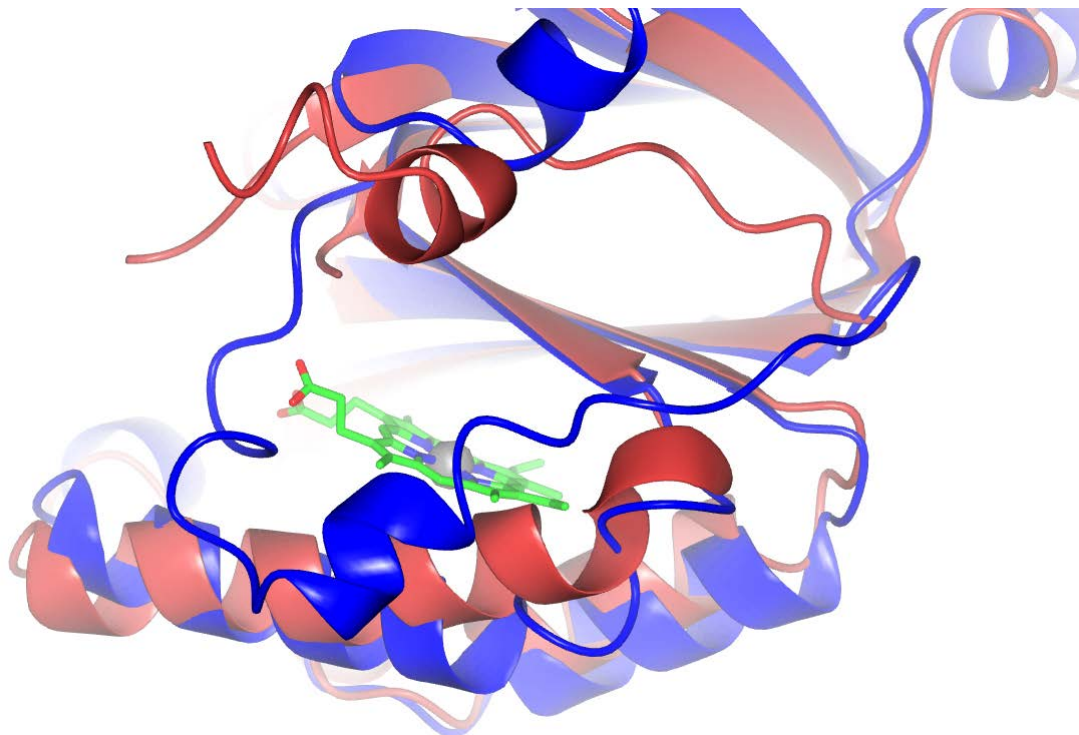


Figure 10: Helix 3' of LmCld clashes with heme; NdCld in red, the helix of LmCld (blue) is tilted in a way that will sterically hinder heme-binding



Moreover, LmCld contains a flexible stretch of aminoacids (residues 111 – 122) that in these data show electron density in 3 out of 5 subunits at low sigma levels. The loop is located at the entrance site of the cavity. Its density cannot be used to build the backbone in compliance with Ramachandran restraints. Probably the loop becomes slightly more ordered at crystallographic interfaces which is the case for these three subunits.

When NdCld was purified *via* Ni-NTA affinity the elution conditions include imidazole which binds to the heme iron and also acts as a weak inhibitor and can be observed in the crystal structure (PDB: 3NN1; (Kostan et al., 2010)). Georg Mlynek (Mlynek, 2010) crystallized the 6x his-tagged construct of LmCld which led to the assumption that these conditions might impair the protein's ability to keep heme bound.

Here the strep-tagged LmCld was crystallized to minimize potential errors caused by chemicals binding to heme.

The protein was expressed, purified and crystallized as described in materials and methods. Diffraction data was collected at BESSY ID 14-1 and the structure was solved to a resolution of 2.21 Å and an $R_{\text{free}} = 0.264$ (see Tables 13 and 14).

Nonetheless, also in this structure no electron density was found at positions where heme is located in homologous structures. There might still be the possibility that in *Listeria monocytogenes* additional factors help incorporating heme that are absent in *E. coli*.

To test whether or not the absence of heme is an artefact of recombinant expression, several mass spectrometry methods and X ray fluorescence were applied to the native LmCld (see section 6.5).

Figure 11: LmCld crystal

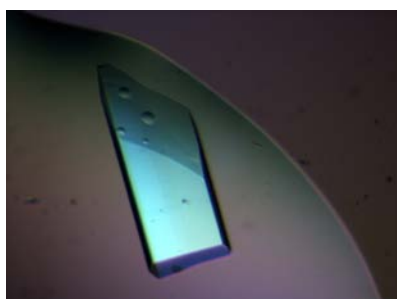


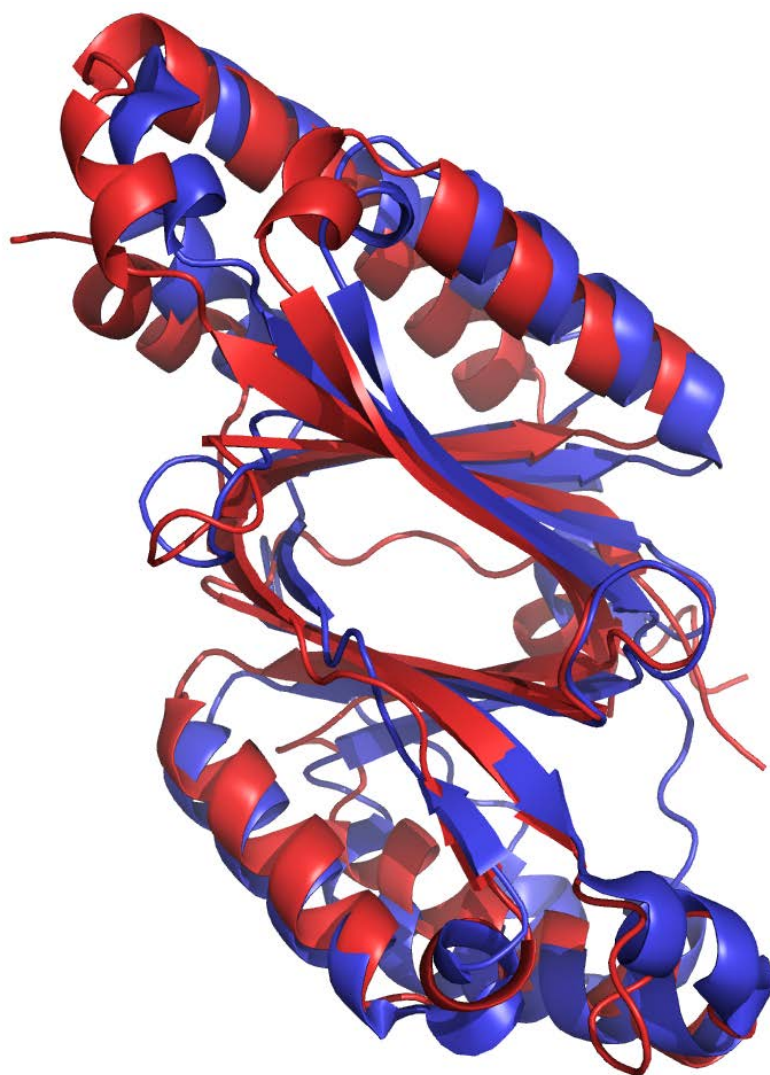
Table 13: Data Collection of LmCld

Source	BESSY ID 14-1
Wavelength	0.918410 Å
Space group	C2
Unit cell	$a = 240.35 \text{ Å}$, $b = 108.68 \text{ Å}$, $c = 78.17 \text{ Å}$; $\beta = 98.9^\circ$
Molecules/a.u.	5
Unique reflections	99212 (16031)
Resolution	46.48 – 2.21 Å (2.34 - 2.21)
Completeness	98.9% (96.0%)
Redundancy	2.6 (2.8)
I/s(I)	7.3 (3.1)
R _{meas}	14.8% (53.1%)
R _{merge}	18.7% (94.4%)

Table 14: Refinement Statistics LmCld

R_{work}	0.240
R_{free}	0.264
RMSD bonds	0.014 Å
RMSD angles	1.172°
Avg. B-factor	40.8 Å ²

Figure 12: Superposition of chain A of LmCld (red) and NdCld (3NN1, blue)



6.3. Structure of LmCld with protamine

The thermal shift assay showed a stabilizing effect of a polypeptide called protamine, a small arginine-rich peptide. When crystallized in the same conditions, the addition of protamine leads to a different crystal packing, i. e. $P2_1$ as compared to $C2$ without the peptide. The peptide itself appears not to be ordered in the crystal, thereby not showing any electron density.

The structure was solved to a resolution of 2.1 Å and superposition with the crystal structure without protamine shows no big difference with an r.m.s.d. of 0.223 Å over the backbone atoms of one chain. In contrast to the structure without protamine, where the flexible loop between residues 110 and 123 could never be modeled, one additional residue (111) in chains B, C and D (residues 111 and 112) and two in chain E could be modeled.

Figure 13: Superposition of LmCld (red) and LmCld-protamine (cyan); r.m.s.d. of backbone atoms = 0.223 Å (834 to 834 atoms)

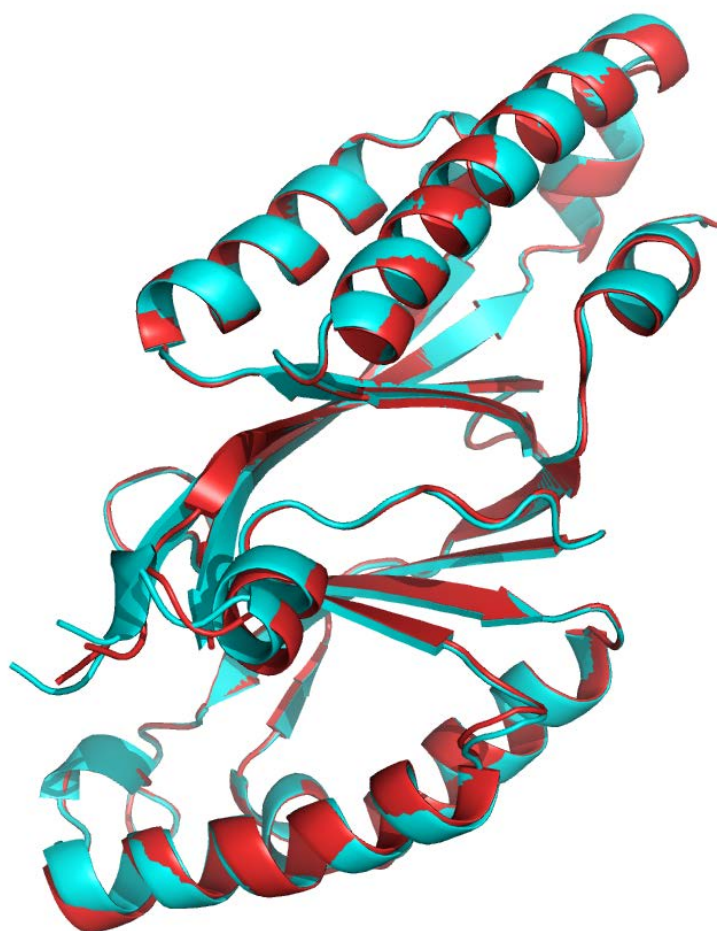


Table 15: Data collection statistics LmCld with protamine

Source	BESSY ID 14-1
Wavelength	0.918410 Å
Space group	P2 ₁
Unit cell	a = 78.06 Å b = 128.40 Å c = 78.22 Å; β = 105.9°
Molecules/a.u.	5
Unique reflections	161585 (17049)
Resolution	37.18 – 2.09 Å (2.15 – 2.09)
Completeness	99.7% (99.9%)
Redundancy	4.19 (4.29)
I/s(I)	6.5 (2.0)
CC1/2	98.2* (70.1*)
R _{meas}	20.3% (79.0%)
Temperature	100 K

Table 16: Refinement statistics LmCld with Protamine

R _{work}	0.217
R _{free}	0.261
RMSD bonds	0.014 Å
RMSD angles	1.452°
Avg B-factor	22.9 Å ²

6.4. LmCld with anomalous scatterers

Most stabilizing compounds identified in the thermal shift assay were divalent cations (see section 6.1). Almost all of them exhibited X-ray absorption at wavelengths close to their absorption edge. By appropriate choice of wavelength their positions in the crystal can be determined by exploiting their anomalous signal.

Of the 14 conditions that increased the thermal stability of LmCld six were chosen for crystallization that covered all the stabilizing components. Additionally, LmCld was co-crystallized with Fe(III) although it did not show stabilizing

effects. In the very sensitive ICP-MS approach traces of iron were detected (see section 6.5.3), that is why it was also selected.

For crystallization conditions see table 9.

The search for a putative cofactor for LmCld by screening additives was based on the assumption that a specific cofactor would bind at specific sites and also stabilize the structure.

Only one additive was found to bind at specific sites, which was Ba^{2+} . For all the other anomalous scatterers the stabilizing effects seems to be unspecific and those could not be located.

Addition of BaCl_2 led to an increase in thermal stability from 53°C to 68°C. Ba^{2+} was found to bind once to each subunit, always in the same position. It replaces a water molecule in the tight turn between β -strands 2 and 3, coordinated by backbone carbonyl-oxygens and by Asp69 (see Figure 14). Since the aspartic acid in this turn is conserved also in other Clds (both validated and non-validated), it can be speculated that those might also be stabilized by Ba^{2+} .

Nonetheless the biological relevance of this binding is probably negligible. The tight turn between beta-strands 2 and 3 is approximately 28 Å away from the conserved histidine, which marks the reaction site for canonical Clds.

At the energy used for these data (6,200 keV, see Table 17) the sulfur atoms are also visible at a sigma level of 4, whereas Ba^{2+} still gives signal above sigma = 8. The anomalous signal for sulfur atoms provides an intrinsic proof of the power of this method.

Figure 14: Location of Ba²⁺ co-crystallized with LmCld contoured at 4 sigma

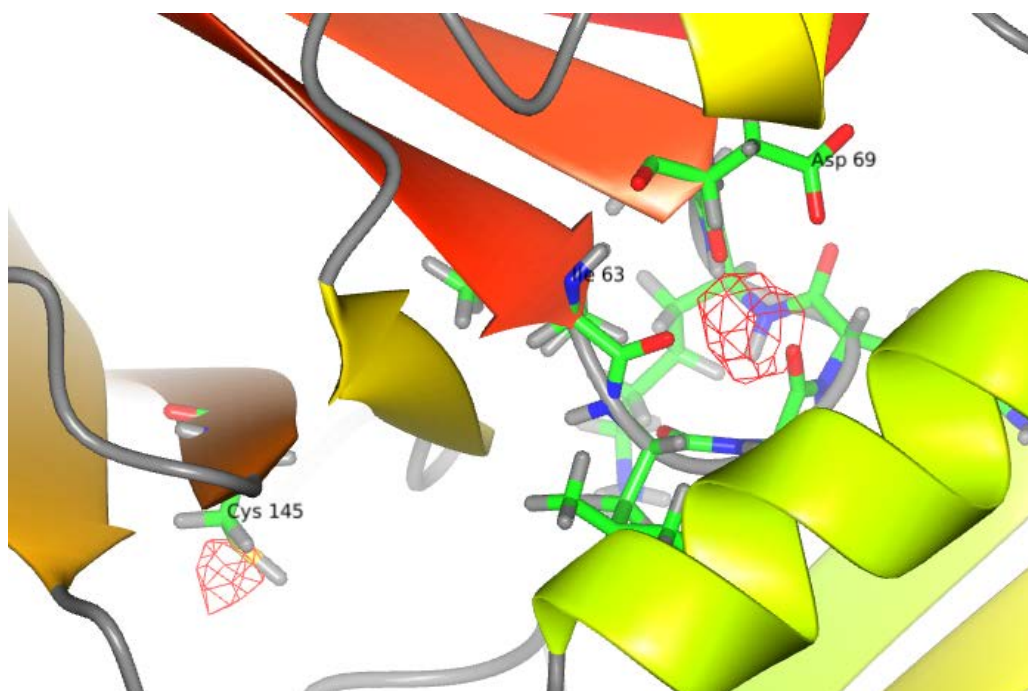


Table 17: Contributions to anomalous scattering of barium and sulfur at 6200 keV

	f'	f''
Barium	-5.75	12.53
Sulfur	0.38	0.89

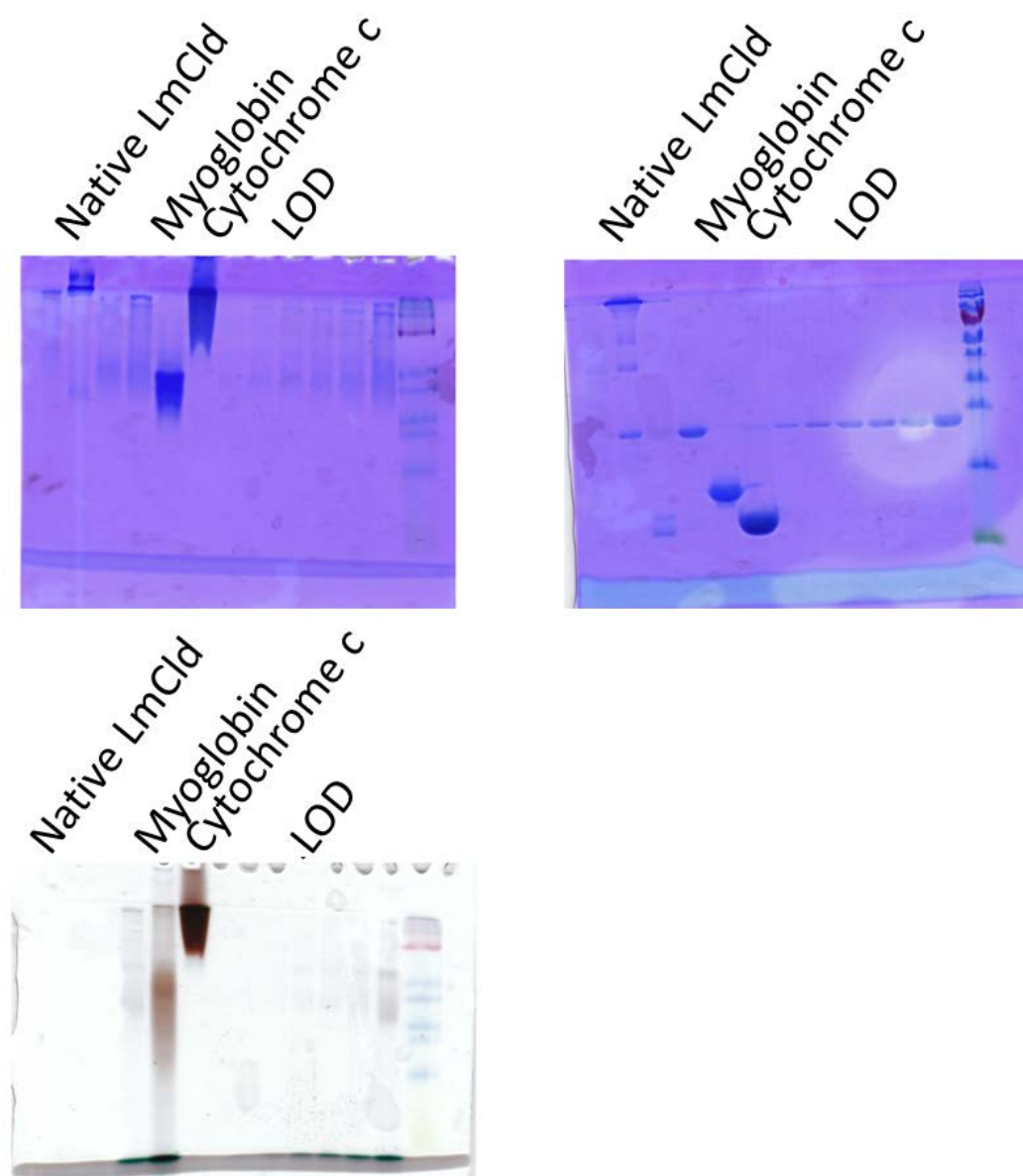
6.5. Native LmCld

LmCld expressed in its natural environment, i. e. in the *Listeria monocytogenes* lab strain LO28, was purified by immuno-precipitation as described in section 5.19. The presence of heme was tested by several means. In order to check for factors that might not be available during recombinant expression in *E. coli* several mass spectrometry approaches and X-ray fluorescence measurement were employed.

6.5.1. Heme-staining of native LmCld

Native LmCld was eluted from the beads in heme-staining sample buffer and run on a polyacrylamide gel with the buffer TBE with subsequent heme staining as described in section 5.20. In parallel the same samples were applied to conventional SDS-PAGE. The absence of SDS in the running buffer TBE results in weak penetration of the separation gel and therefore weak separation. Nonetheless the method is very sensitive with a limit of detection of 40 pmol heme. This was confirmed by a dilution series of NdCld (on the right part of the gels). Heme migrates at the dye front and appears green after the staining procedure. Comparing the protein amounts needed for sufficient signal, the immuno-precipitated LmCld in lane annotated "Native LmCld" would give a high signal if heme was actually bound, even at a low ratio. For comparison also myoglobin with non-covalently bound heme and cytochrome c covalently bound to heme were applied.

Figure 15: Heme-staining of native LmCld; top left: Coomassie blue staining after heme-staining (bottom, same gel); top right: same samples in conventional SDS-PAGE

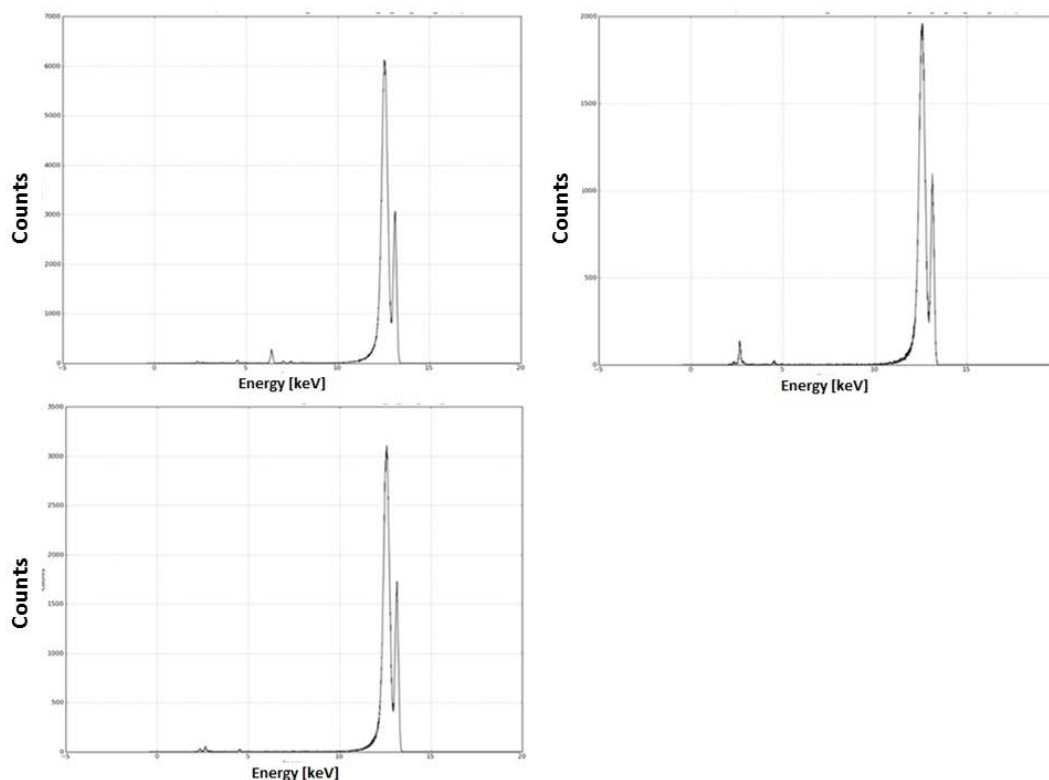


6.5.2. X Ray Fluorescence

The spectra of eluted native LmCld, recombinant LmCld and NdCld were collected at ESRF on ID 14-4 by Sandor Brockhauser. NdCld shows peaks at Fe-edges (at 6.4 and 7.1 keV, see Figure 16) whereas neither native nor recombinant LmCld does. LmCld samples show peaks at 2.62 keV which indicates the not surprising presence of chlorine (LmCld in TBS and NdCld in HEPES buffer). All samples show peaks for sulfur at 2.3 keV, possibly calcium at 3.69

keV, as well as an indication to the presence of possibly titanium, iodine or tellurium at 4.51 keV.

Figure 16: X ray fluorescence spectra of NdCld (top left), recombinant LmCld (top right) and native LmCld (bottom)



6.5.3. Inductively Coupled Plasma Mass spectrometry

A more sensitive method to detect trace elements is ICP-MS (Kretschy et al., 2012). The ionization process atomizes the sample and can in principle detect any element heavier than nitrogen. Measurements were done at BOKU Vienna, Department for Analytical Chemistry (special thanks to Stephan Hann and group for advice in sample preparation and measurements).

Native LmCld, due to the immuno-precipitation together with IgG, was measured after a SEC column which removed trace elements only present in the buffer and not binding to the protein. Intriguingly, co-eluting with the peak of sulfur (measured as its oxide ^{48}SO ; which indicates presence of protein) iron was detected (see Figure 18). This was not the case when only IgG was measured as a negative control (see Figure 17).

Figure 17: ^{48}SO IgG negative control SEC-ICP-MS

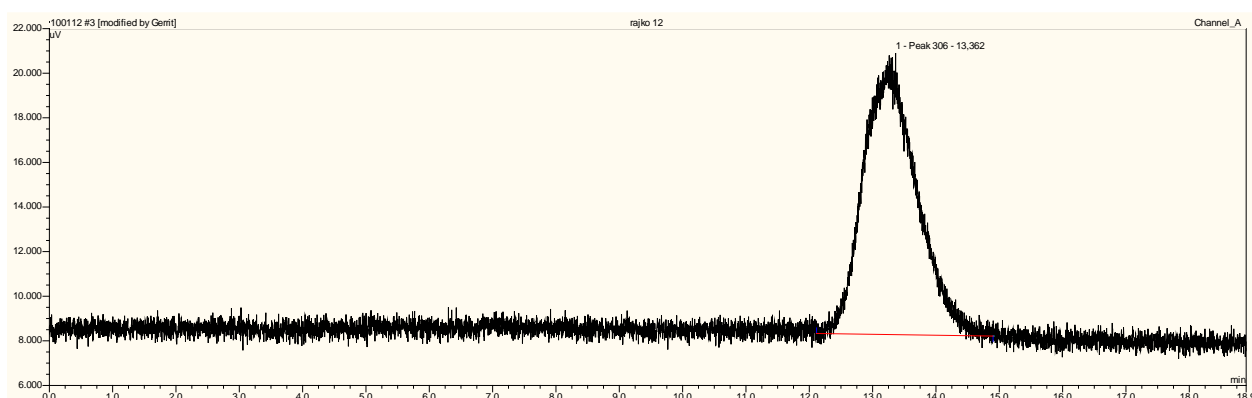
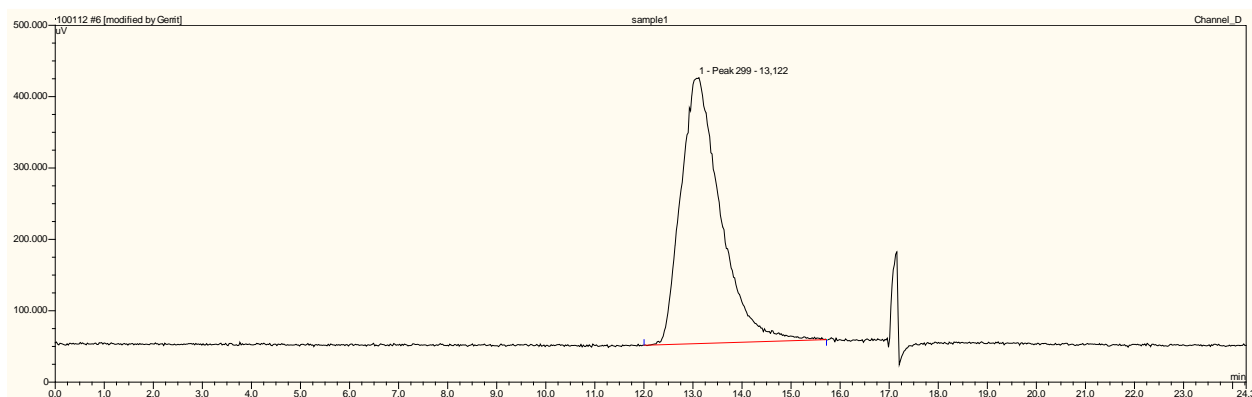


Figure 18: ^{56}Fe trace of native LmCld SEC-ICP-MS



At a retention time of 13.1 min a high signal of iron was detected. Considering the retention time of IgG of 13.4 min this indicates to be the target LmCld together with IgG. Low signals of cobalt and aluminum were also detected (not shown).

6.5.4. Hydrophobic cofactor mass spectrometry

An approach to identify a cofactor that fits the hydrophobic active site cavity and confirm the absence of heme was to scan all components present in the sample by nanoESI-MSMS (BSRC Mass Spectrometry and Proteomic Facility St. Andrews). Native LmCld was digested off the beads with trypsin and the sample applied to a reverse phase column, on-line with nESI. The expected monoisotopic mass of heme is 616 m/z which gave no significant signal (Figure 19). Figure 20 shows the total ion count of the whole run. The extracted masses could not be assigned to a known cofactor.

Spectrum in region of expected mass of heme

Mass spectrum showing intensity (counts) versus m/z ratio. The spectrum displays several peaks, with the most prominent ones labeled with their m/z values: 610.04, 612.04, 614.04, 615.20, 616.20, 617.20, 619.20, 632.03, and 634.02. The x-axis ranges from 600 to 634 m/z , and the y-axis ranges from 0.0 to 16.0 counts.

TIC: from Andreas.LmCldwell

Max: 7.9e5

Intensity, cps

Time, min

Peaks labeled with retention times (min):

- 261.15
- 186.15
- 472.26
- 319.12
- 144.06
- 122.00
- 972.42
- 762.05
- 863.82
- 300.15
- 323.08
- 323.09
- 1171.85
- 133.06
- 323.08
- 988.44
- 449.12
- 449.12
- 398.25
- 317.16
- 536.26
- 536.25
- 536.25

Continuing the work of Kira Gysel (Gysel, 2011), another interesting NdClD mutant was crystallized and its structure determined by X ray diffraction. The putative electron donor Trp145 was mutated to phenylalanine and its steady-state kinetics indicate that substrate binding is not hindered yet the catalytic efficiency suffers substantially from this mutation (Hofbauer, unpublished data). This decrease in activity is not caused by alteration of the structure, the phenylalanine is in the same plane as the tryptophan in the wildtype structure (see Figure 21).

Page 55 of 77

Again the observation that despite being structurally highly similar (r.m.s.d. of backbone atoms = 0.265 Å (867 to 867 atoms)) to the wildtype structure the resolution does not exceed 2.8 Å (compared to 1.8 Å of the wildtype structure) when $I/\sigma(I)$ is used as the cut-off parameter.

Here the XDS parameter C1/2 (Karplus and Diederichs, 2012) was used and made it possible to reach a slightly higher resolution of 2.58 Å at $R_{\text{free}} = 0.27$.

Figure 21: NdCld W145F (3NN1, blue) superposed with wildtype NdCld (green)

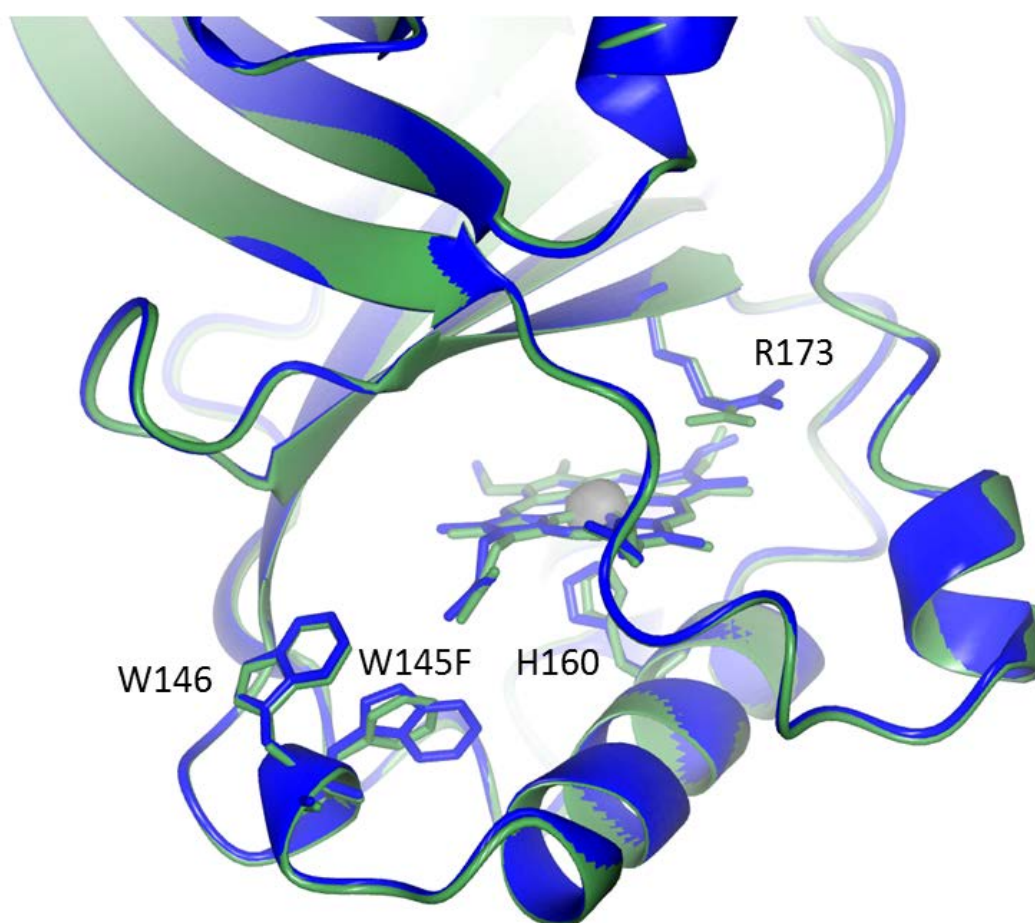


Table 18: Data collection statistics of NdCld W145F

Source	ESRF ID 23-1
Wavelength	0.8726 Å
Space group	C2
Unit cell	$a = 138.30 \text{ Å}$ $b = 112.62 \text{ Å}$ $c = 120.32 \text{ Å}$; $\beta = 118.48^\circ$
Molecules/a.u.	5
Unique reflections	40277 (2503)
Resolution	43.55 – 2.76 Å (2.83 - 2.76)
Completeness	96.2% (81.3%)
Redundancy	3.24 (2.19)
I/s(I)	15.3 (0.7)
CC1/2	99.9* (44.0*)
R _{meas}	6.8% (134.8%)
Temperature	100 K

Table 19: Refinement statistics of NdCld W145F

R _{work}	0.197
R _{free}	0.229
RMSD bonds	0.013 Å
RMSD angles	1.489°
Avg B-factor	79.7 Å ²

6.7. Structure of NdCld W145F in complex with cyanide

The structure of NdCld W145F was also solved in complex with its inhibitor cyanide. Surprisingly the addition of inhibitor did not improve the statistics, still the two structures are highly similar with an r.m.s.d. = 0.230 Å (881 to 881 atoms).

Table 20: Data collection statistics of NdCld W145F with cyanide

Source	ESRF ID 23-1
Wavelength	0.8726 Å
Space group	C2
Unit cell	$a = 136.16 \text{ Å}$ $b = 113.40 \text{ Å}$ $c = 118.80 \text{ Å}$; $\beta = 117.9^\circ$
Molecules/a.u.	5
Unique reflections	45519 (1672)
Resolution	43.45 – 2.58 Å (2.64 - 2.58)
Completeness	89.9%% (44.8%)
Redundancy	7.19 (3.63)
I/s(I)	10.2 (0.4)
CC1/2	99.8* (13.7*)
R _{meas}	14.9% (376.7%)
Temperature	100 K

Table 21: Refinement statistics of NdCld W145F with cyanide

R _{work}	0.214
R _{free}	0.269
RMSD bonds	0.015 Å
RMSD angles	1.644°
Avg B-factor	85.1 Å ²

6.8. Oligomeric state of different Clds

The M_W and therefore the oligomeric state of various Clds was measured as described in section 5.25. Mlynek et al. (Mlynek et al., 2011) solved the structure of NwCld which is a truncated version of active Cld by X ray diffraction and found it to be dimeric. Kira Gysel (Gysel, 2011) reported the hexameric structure of apoNdCld whereas the holoform wildtype and mutants are arranged as pentamers in the crystal. To test whether these findings were crystallographic artefacts the M_W in solution was monitored by SLS. This was done

in collaboration with Kira Gysel and also reported in her Diploma Thesis (Gysel, 2011).

The newly purified SsCld was found to elute close to the void volume on an Superdex200 16/60 SEC column. Compared to pentameric NdCld this indicates a higher oligomeric state. To measure the exact M_W SsCld was also applied to SLS.

The M_W of NwCld in solution corresponds to the expected dimeric M_W (Figure 22) of approximately 45 kDa. ApoNdCld appears in solution as a pentamer with $M_W = 135$ kDa (Figure 23), meaning that the hexameric crystal structure was caused by the crystallization conditions. SsCld on the other hand was found to have a M_W between 210 and 220 kDa corresponding to at least a heptameric or even octameric organization (would be ca 230 kDa).

Although no heptameric or octameric structure has been reported by now, it can be speculated that higher oligomerization is important for stability. Hofbauer et al. (Hofbauer S, 2012) reported a large difference in thermal stability between the dimeric NwCld ($T_M = 53^\circ\text{C}$) and the pentameric NdCld ($T_M = 92^\circ\text{C}$). The thermophile archaeon *Sulfolobus solfataricus* grows optimally at 80°C (Zaparty et al., 2010), at this temperature requiring high thermostability for all its components.

Figure 22: SLS profile of dimeric NwCId (Gysel, 2011)

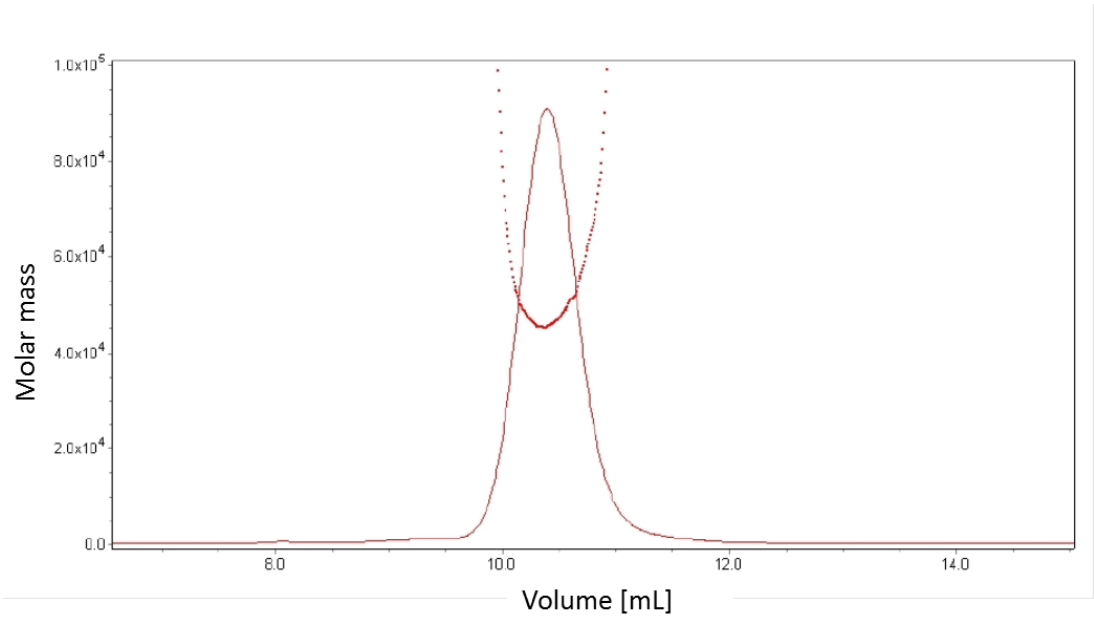


Figure 23: SLS profile of pentameric apoNdCId (Gysel, 2011)

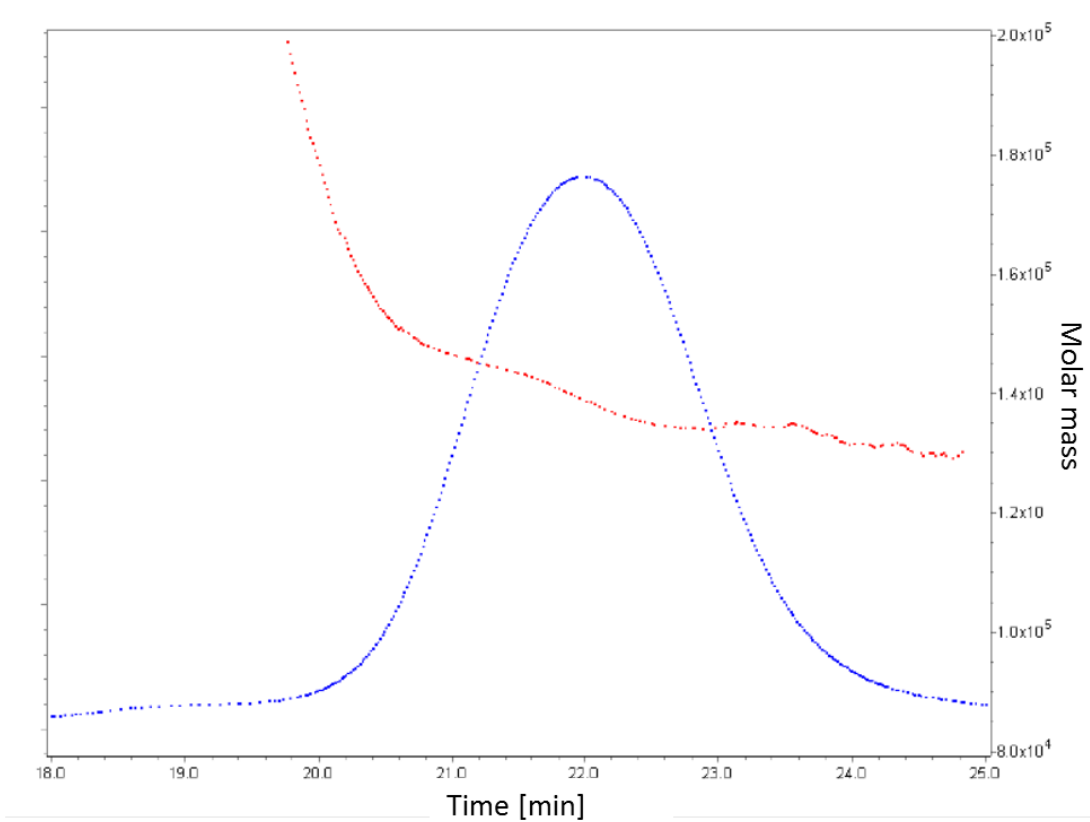
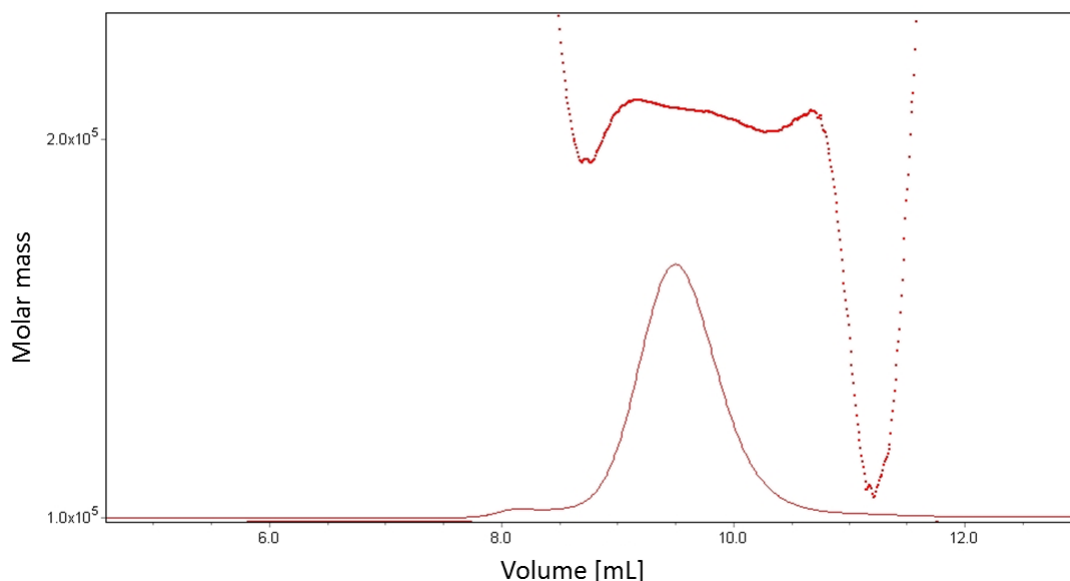


Figure 24: SLS profile of SsCld

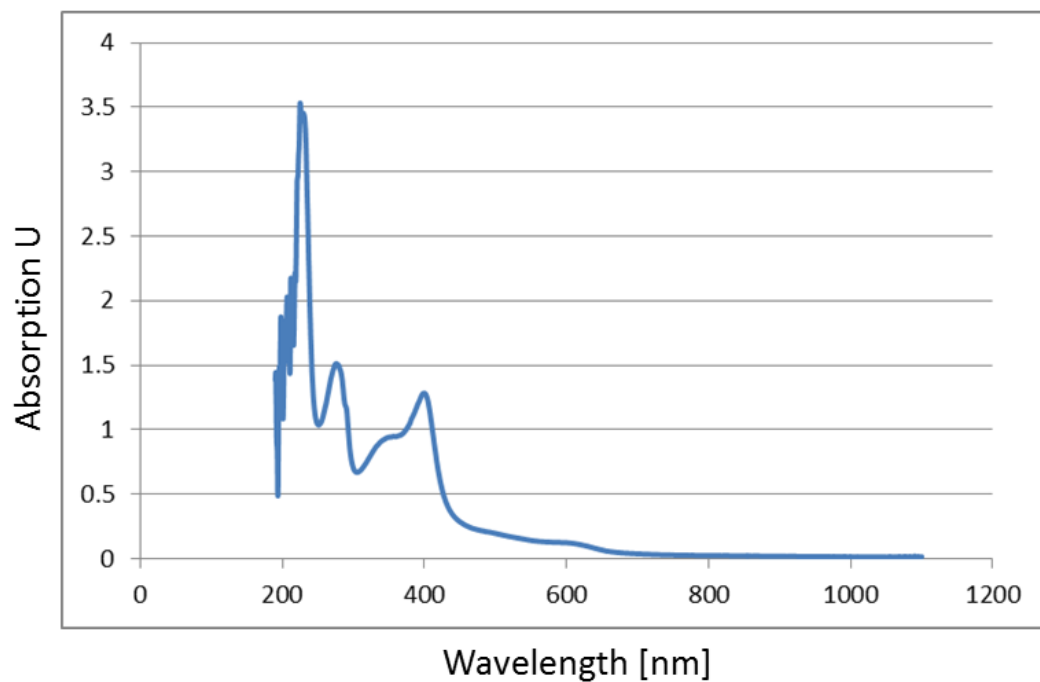


6.9. Heme content of SsCld

The Reinheitszahl RZ of heme-binding proteins can be determined by UV-vis spectroscopy. It is defined as A_{soret}/A_{280} and reflects the ratio in which heme binds to the protein. The theoretical Reinheitszahl (100% heme occupation) of SsCld is 1.6, the Soret peak is at 401 nm and the RZ was determined to be 1.3 (see Figure 25) meaning that 82% of the proteins subunits are occupied with heme. The Soret peak is red-shifted compared to NdCld with a Soret maximum at 408 nm, indicating a different heme environment.

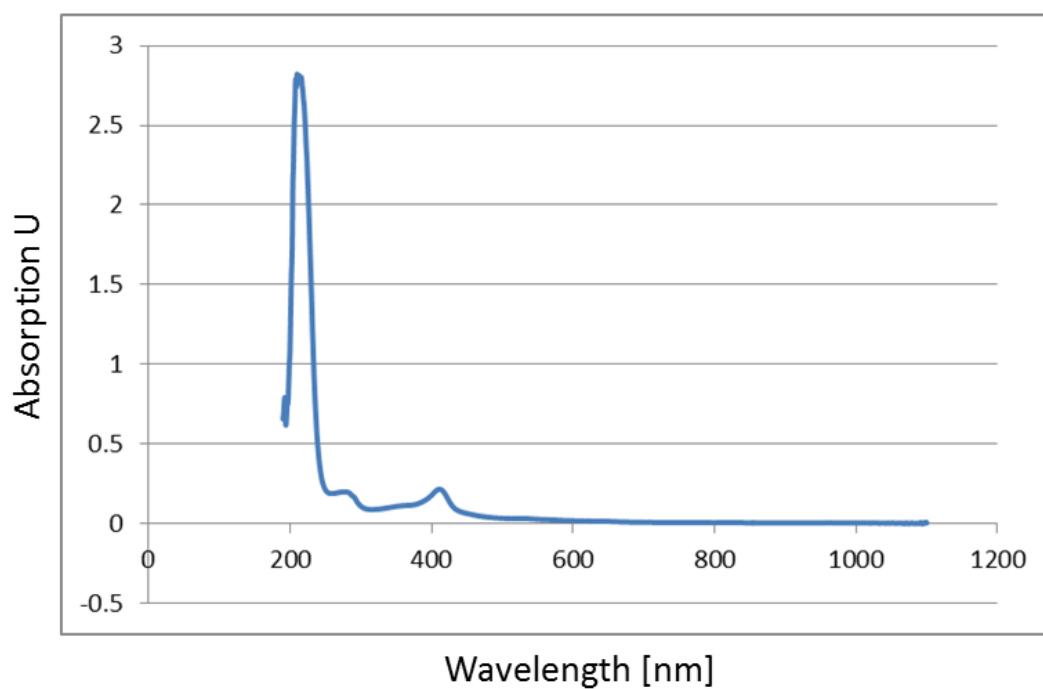
Reduction of SsCld by addition of dithionite results in a shift of the Soret maximum from 401 nm to 417 nm. Similar soret maxima of reduced and oxydized heme proteins have been reported (Maixner et al., 2008; Stenklo et al., 2001; van Ginkel, 1996).

Figure 25: UV-vis spectrum of SsCld



For comparison, the UV-vis spectrum of NdCld was taken.

Figure 26: UV-vis spectrum of NdCld



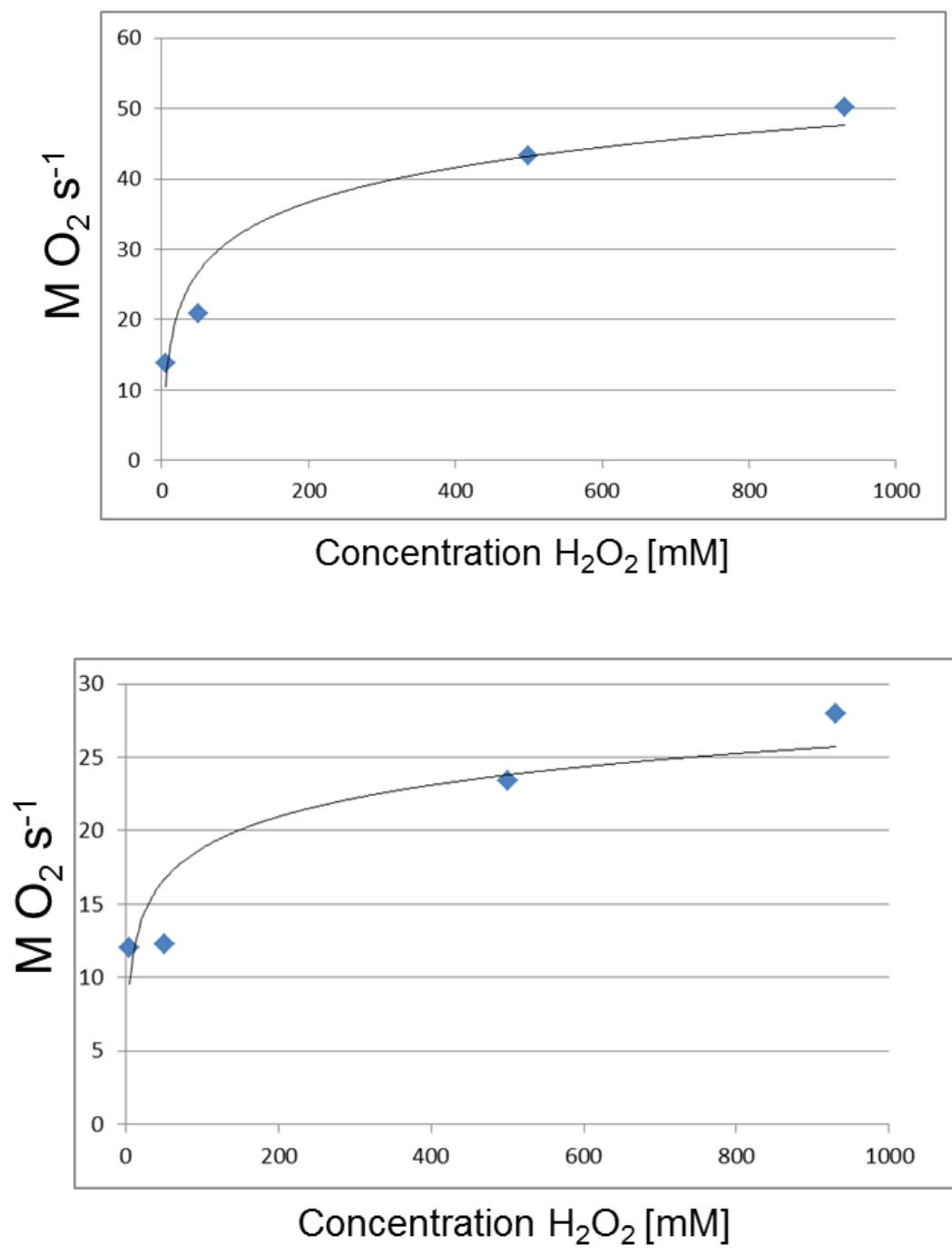
6.10. Steady-state kinetics

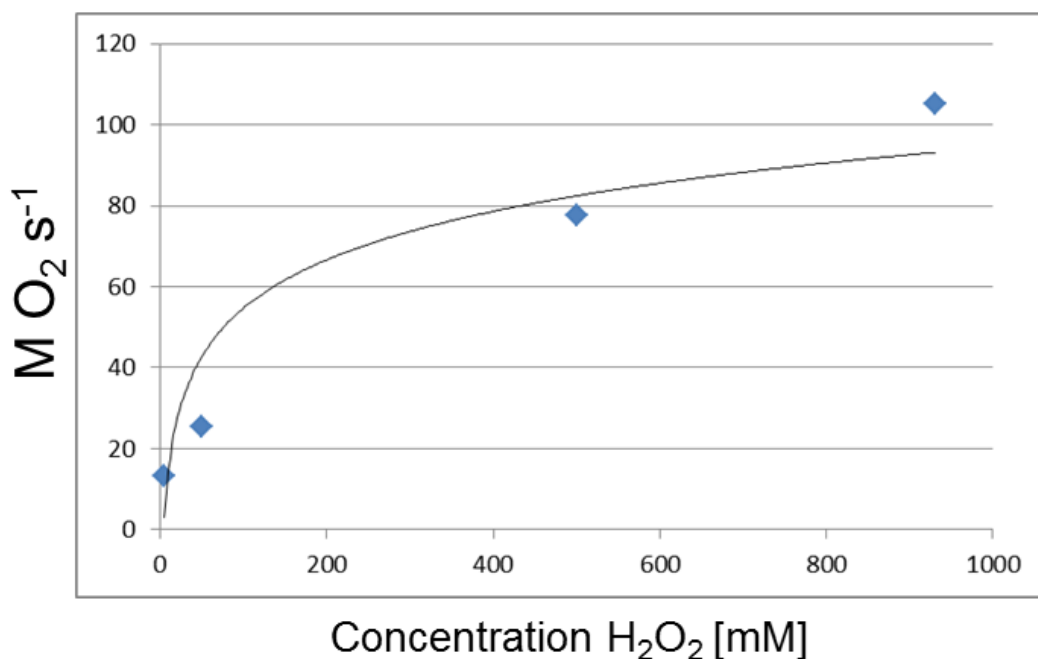
The function of Cld-like proteins is still not known. A representative of the archaeal phylum containing a serine residue instead of arginine in active Clds is SsCld. The protein was purified as described in section 5.15, its heme content determined (see section 6.9) and its Cld- and catalase-activity was measured (see Section 6.10).

SsCld, lacking the key residue arginine of active Clds, showed no production of molecular oxygen when the substrate chlorite was added. Since the measurements were taken at 35°C, residual Cld-activity might still play a small role at the optimal temperature of *Sulfolobus solfataricus* growth (80°C). Due to the experimental requirements of the Clark-type electrode the highest temperature available (45°C) was used from this point on.

When adding H₂O₂ as a substrate at 45°C, O₂ production can be observed in a concentration- and pH-dependent manner. This means that the reaction is being catalyzed by SsCld, although the production rate is still weak compared to canonical catalases. The highest activity was measured at pH 9 (see figure 27). Again, this weak activity might get stronger when approaching the natural habitat's temperature of *Sulfolobus solfataricus*. K_{cat} and K_{M} were not calculated because of too few data points.

Figure 27: Temperature- and pH-dependent catalase activity of SsCld; Oxygen release plotted against H₂O₂ concentration Top: pH 5.5; middle pH 6.25; bottom: pH 9





6.10. Steady-state kinetics of the NdCld mutant W145F

The enzymatic parameters of NdCld W145F were measured by Stefan Hofbauer as described in section 5.24.

Table 22: Comparison of steady-state kinetics of active Clds and mutants

Protein	K_M [μM]	K_{cat} [s^{-1}]	K_{cat}/K_M [$\text{M}^{-1} \text{s}^{-1}$]	
NdCld (wt) + imidazole	58 +/- 37	35	6.0×10^5	(Kostan et al., 2010)
NdCld (wt)	52 +/- 7	42	8.1×10^5	Hofbauer, Gysel
NdCld W145F	172 +/- 10	20	1.2×10^5	Hofbauer, Hagmüller
Azospira oryzae GR1 Cld	170	1200	7.1×10^6	(van Ginkel, 1996)

The mutation of the putative electron donor Trp145 to phenylalanine does not hinder substrate binding. The turnover rate however suffers from this exchange and K_{cat}/K_M drops five fold. This could be the result of decreased availability of electrons necessary for the reaction.

7. Discussion

The function of Cld-like proteins is still an open question. With the representative of the lineage including human pathogens, Cld-like protein from *Listeria monocytogenes*, it was first shown that heme is not a cofactor even in *Listeria monocytogenes* itself and that the absence of this prosthetic group in crystal structures is no artefact of recombinant production. Mimicking the active site of LmCld (W146Y and R173Q) in the active Cld from *Nitrospira defluvii* drops the enzymatic activity but this double mutant is still able to decompose chlorite probably due to the ability to bind heme (Gysel, 2011). The absence of heme in LmCld is most likely caused by the tilting of alpha-helix 3' and other residues that sterically hinder heme binding (Y147, G178, I215, M219; see section 6.2). Although the results presented here may seem contradictory, as XRF did not show presence of iron but the more sensitive method ICP-MS did, the mass over charge ration (m/z) of heme was never observed in any mass spectrometry measurement of native LmCld. Apart from that, no heme could be detected by heme-staining of native LmCld. In addition, neither a mass shift for covalently bound heme nor other post translational modifications of native LmCld was found. The origin of the signal for elemental iron in ICP-MS remains unclear and will need complementary methods to be proved since it apparently does not stem from heme. The related Cld from *Thermus thermophilus*, which also contains a glutamine key residue, could be reconstituted with heme (60% of subunits loaded when reconstituted at high temperatures) and shows then a weak Cld- and catalase-activity (Ebihara et al., 2005). This suggests that probably the whole "glutamine-cluster" of Clds might not bind heme and have a different function.

The screening for potential cofactors with recombinant LmCld was not successful, though general aspects of the correlation between crystallizability and thermal stability can be considered. Dupuex et al. (Dupuex F, 2011) reported increased likelihood for crystallization of proteins when crystallized in buffer conditions that elevated the protein's melting temperature. The statistics of LmCld and LmCld co-crystallized with the poly-cationic peptide protamine reveal that if better diffraction data is required, screening additives and different buffer conditions to increase thermal stability might be worth a try. For example, the overall atomic displacement parameters (or average B factors) of the LmCld-protamine structure are only half the value of LmCld crystallized alone. Yet the flexible loop from residues 111 – 123 was still not ordered in the protamine structure although in 3 of chains one residue more and in one chain two residues more could be modeled in agreement with the observed electron density in compliance with Ramachandran restraints.

The coordination of the barium ion in the tight turn between β strand 2 and 3 seems to be the only specific interaction mediated by divalent cations that are able to stabilize LmCld. The turn is made up by 5 residues and the ion is probably coordinated by backbone carbonyl-oxygens and the side chain oxygen of aspartic acid. If iron binds to the protein not as part of heme it would probably also be coordinated by “hard chelators” like the backbone carbonyl-oxygens. Still the biological function of such an interaction will be hard to interpret and the conservation of the cavity and the coordinating histidine have to be taken into consideration. The aspartic acid involved in Ba^{2+} coordination is conserved over many Clds and Cld-like proteins, providing means for potential stabilization and increased crystallizability also of other Clds.

LmCld was found to exhibit weak catalase-activity, too (Füreder, 2009). Due to the presence of canonical catalase in *Listeria monocytogenes* this function is probably negligible. Here we present weak catalase-activity of SsCld which in contrast to LmCld is able to bind heme. Intriguingly, all archaea containing a *cld*-gene are aerobic and do not have a gene for canonical catalase (Christa Schleper, personal correspondence). To test the activity at the temperature of optimal growth for *Sulfolobus solfataricus* a different protocol for measuring catalase-activity at high temperatures will have to be employed. The higher order in oligomerization of SsCld will have to be confirmed by complementary methods like X-ray diffraction structural analysis and the properties of the subunit-interfaces revealed might answer how higher oligomerization can influence the protein's stability. This would expand the results of (Hofbauer S, 2012).

The structure of mutated NdCld reported in this thesis is more of a confirmation that the decrease in enzymatic activity is not caused by structural deviations but by the decreased availability of electrons needed for the Cld-reaction. With this mutant it was possible to monitor the reaction since the turnover rate is much lower but binding of substrate is not impaired. It was possible to spectroscopically observe the intermediate state and also to induce the reaction when starting with the intermediate hypochlorite (Stefan Hofbauer, personal correspondence). The goal for crystallographers to trap the intermediate in a crystal will still be difficult due to remaining activity and resulting bleaching also with this mutant.

8. References

- Adams, P.D., Afonine, P.V., Bunkoczi, G., Chen, V.B., Davis, I.W., Echols, N., Headd, J.J., Hung, L.W., Kapral, G.J., Grosse-Kunstleve, R.W., *et al.* (2010). PHENIX: a comprehensive Python-based system for macromolecular structure solution. *Acta crystallographica Section D, Biological crystallography* 66, 213-221.
- Bender, K.S., O'Connor, S.M., Chakraborty, R., Coates, J.D., and Achenbach, L.A. (2002). Sequencing and transcriptional analysis of the chlorite dismutase gene of *Dechloromonas agitata* and its use as a metabolic probe. *Applied and environmental microbiology* 68, 4820-4826.
- Brandon R. Goblirsch, B.R.S., Jennifer L. DuBois, and Carrie M. Wilmot (2010). Structural features promoting dioxygen production by *Dechloromonas aromatica* chlorite dismutase. *J Biol Inorg Chem* 15(6), 879–888.
- Coates, J.D., Achenbach, L. A. (2004). Microbial perchlorate reduction: rocketfueled metabolism. *Nat Rev Microbiol* 2004 Jul;2(7):. 569-580.
- Collaborative Computational Project, N. (1994). The CCP4 Suite: Programs for Protein Crystallography. *Acta Cryst D* 50, 760-763
- Dupeux F, R.M., Seroul G, Blot D, Márquez JA. (2011). A thermal stability assay can help to estimate the crystallization likelihood of biological samples. *Acta Crystallogr D Biol Crystallogr* 67(Pt 11), 915-919.
- Ebihara, A., Okamoto, A., Kousumi, Y., Yamamoto, H., Masui, R., Ueyama, N., Yokoyama, S., and Kuramitsu, S. (2005). Structure-based functional identification of a novel heme-binding protein from *Thermus thermophilus* HB8. *J Struct Funct Genomics* 6, 21-32.
- Emsley, P., Lohkamp, B., Scott, W. G., and Cowtan, K. (2010). Features and development of coot. *Acta crystallographica Section D, Biological crystallography* 66(Pt 4), 486–501.
- Ettwig, K.F., Butler, M.K., Le Paslier, D., Pelletier, E., Mangenot, S., Kuypers, M.M., Schreiber, F., Dutilh, B.E., Zedelius, J., de Beer, D., *et al.* (2010). Nitrite-driven anaerobic methane oxidation by oxygenic bacteria. *Nature* 464, 543-548.
- Francis RT Jr, B.R. (1984). Specific indication of hemoproteins in polyacrylamide gels using a double-staining process. *Anal Biochem* 136(2):, 509-514.
- Füreder, S. (2009). PhD Thesis: Functional analyses of chlorite dismutase-like proteins from *Listeria monocytogenes* and *Nitrobacter winogradskyi*
- Gasteiger E, H.C., Gattiker A, Duvaud S, Wilkins MR, Appel RD *et al* (2005). Protein identification and analysis tools on the ExPASy server. Walker JM (ed) *The proteomics protocols handbook* Humana Press, 571-607.
- Goblirsch, B., Kurker, R.C., Streit, B.R., Wilmot, C.M., and DuBois, J.L. (2011). Chlorite dismutases, DyPs, and EfeB: 3 microbial heme enzyme families comprise the CDE structural superfamily. *Journal of molecular biology* 408, 379-398.
- Gysel, K. (2011). Diploma Thesis: Functional and structural studies on chlorite dismutase from *Nitrospira defluvii*.
- Hagedoorn, P.L., De Geus, D. C., and Hagen, W. R. (2002). Spectroscopic characterization and ligand-binding properties of chlorite dismutase from the chlorate respiring bacterial strain gr-1. *Eur J Biochem* 269(19), 4905–4911.
- Hanahan, D. (1983). Studies on transformation of *Escherichia coli* with plasmids. *Journal of molecular biology* 166, 557-580.
- Hofbauer, S., Bellei, M., Sundermann, A., Pirker, K.F., Hagmuller, A., Mlynek, G., Kostan, J., Daims, H., Furtmuller, P.G., DjinoVIC-Carugo, K., *et al.* (2012). Redox thermodynamics of high-spin and low-spin forms of chlorite dismutases with diverse subunit and oligomeric structures. *Biochemistry* 51, 9501-9512.

Hofbauer S, G.K., Mlynek G, Kostan J, Hagmüller A, Daims H, Furtmüller PG, Djinić-Carugo K, Obinger C (2012). Impact of subunit and oligomeric structure on the thermal and conformational stability of chlorite dismutases. *Biochim Biophys Acta* 1824, 1031-1038.

Kabsch, W. (2010). Xds. *Acta Crystallogr D Biol Crystallogr* 66, 125-132.

Karplus, P.A., and Diederichs, K. (2012). Linking crystallographic model and data quality. *Science* 336, 1030-1033.

Kengen, S.W., Rikken, G. B., Hagen, W. R., van Ginkel, C. G., and Stams, J., A. (1999). Purification and characterization of (per)chlorate reductase from the chlorate-respiring strain gr-1. *J Bacteriol* 181(21), 6706–6711.

Kostan, J., Sjöblom, B., Maixner, F., Mlynek, G., Furtmüller, P.G., Obinger, C., Wagner, M., Daims, H., and Djinić-Carugo, K. (2010). Structural and functional characterisation of the chlorite dismutase from the nitrite-oxidizing bacterium "Candidatus Nitrospira defluvii": identification of a catalytically important amino acid residue. *Journal of structural biology* 172, 331-342.

Kretschy, D., Koellensperger, G., and Hann, S. (2012). Elemental labelling combined with liquid chromatography inductively coupled plasma mass spectrometry for quantification of biomolecules: a review. *Analytica chimica acta* 750, 98-110.

Lee, A.Q., Streit, B. R., Zdzilla, M. J., Abu-Omar, M. M., and DuBois, J. L. (2008). Mechanism of and exquisite selectivity for o-o bond formation by the heme-dependent chlorite dismutase. *Proc Natl Acad Sci U S A* 105(41), 15654–15659.

Long, F., Vagin, A.A., Young, P., and Murshudov, G.N. (2008). BALBES: a molecular-replacement pipeline. *Acta crystallographica Section D, Biological crystallography* 64, 125-132.

Lucker, S., Wagner, M., Maixner, F., Pelletier, E., Koch, H., Vacherie, B., Rattei, T., Dams, J.S., Spieck, E., Le Paslier, D., *et al.* (2010). A Nitrospira metagenome illuminates the physiology and evolution of globally important nitrite-oxidizing bacteria. *Proc Natl Acad Sci U S A* 107, 13479-13484.

Maixner, F., Wagner, M., Lucker, S., Pelletier, E., Schmitz-Esser, S., Hae, K., Spieck, E., Konrat, R., Le Paslier, D., and Daims, H. (2008). Environmental genomics reveals a functional chlorite dismutase in the nitrite-oxidizing bacterium 'Candidatus Nitrospira defluvii'. *Environmental microbiology* 10, 3043-3056.

Mlynek, G. (2010). Diploma Thesis: Differences within the superfamily of Chlorite Dismutases: structural and functional characterization.

Mlynek, G., Sjöblom, B., Kostan, J., Fureder, S., Maixner, F., Gysel, K., Furtmüller, P.G., Obinger, C., Wagner, M., Daims, H., *et al.* (2011). Unexpected diversity of chlorite dismutases: a catalytically efficient dimeric enzyme from Nitrobacter winogradskyi. *J Bacteriol* 193, 2408-2417.

Murphy, R.M. (1997). Static and dynamic light scattering of biological macromolecules: what can we learn? *Current opinion in biotechnology* 8, 25-30.

Murshudov, G.N., Skubak, P., Lebedev, A.A., Pannu, N.S., Steiner, R.A., Nicholls, R.A., Winn, M.D., Long, F., and Vagin, A.A. (2011). REFMAC5 for the refinement of macromolecular crystal structures. *Acta Crystallogr D Biol Crystallogr* 67, 355-367.

Reinhard L, M.H., Geerlof A, Mueller-Dieckmann J, Weiss MS (2013). Optimization of protein buffer cocktails using Thermofluor. *Acta Crystallogr Sect F Struct Biol Cryst Commun* 69(Pt 2); 209-214.

Renger, G., and Renger, T. (2008). Photosystem II: The machinery of photosynthetic water splitting. *Photosynthesis research* 98, 53-80.

Stenklo, K., Thorell, H.D., Bergius, H., Aasa, R., and Nilsson, T. (2001). Chlorite dismutase from Ideonella dechloratans. *Journal of biological inorganic chemistry : JBIC : a publication of the Society of Biological Inorganic Chemistry* 6, 601-607.

- Ueno, H., K. Oishi, Y. Sayato, and K. Nakamuro (2000). Oxidative cell damage in Kat-sod assay of oxyhalides as inorganic disinfection by-products and their occurrence by ozonation. *Arch Environ Contam Toxicol* 38, 1-6.
- Urbansky, E. (1998). Perchlorate chemistry: implications for analysis and remediation. *Bioremediation Journal* 2(2); 81–95.
- Urbansky, E.T. (2002). Perchlorate as an environmental contaminant. *Environ Sci Pollut Res Int* 9(3); 187–192.
- van Ginkel, C.G., G.B. Rikken, A.G. Kroon, and S.W. Kengen (1996). Purification and characterization of chlorite dismutase: a novel oxygen-generating enzyme. *Arch Microbiol* 166, 321-326.
- Wu, D., He, P., Xu, X., Zhou, M., Zhang, Z., and Houda, Z (2008). The effect of various reaction parameters on bioremediation of perchlorate-contaminated water. *J Hazard Mater* 150(2), 419–423.
- Zaparty, M., Esser, D., Gertig, S., Haferkamp, P., Kouril, T., Manica, A., Pham, T.K., Reimann, J., Schreiber, K., Sierocinski, P., *et al.* (2010). "Hot standards" for the thermoacidophilic archaeon *Sulfolobus solfataricus*. *Extremophiles : life under extreme conditions* 14, 119-142.

9. List of Figures

- Figure 1:** Perchlorate reduction pathway
- Figure 2:** Phylogeny tree of the chlorite dismutase family
- Figure 3:** Ferredoxin-like fold
- Figure 4:** Superposition of chain A of NdCld with LmCld
- Figure 5:** Reaction mechanism of Cld
- Figure 6:** Thermofluor of LmCld with Additive Screen
- Figure 7:** Thermofluor of LmCld with Silver Bullets
- Figure 8:** Thermofluor of LmCld with Silver Bullets Bio
- Figure 9:** Residues of LmCld clashing with heme
- Figure 10:** Helix 3' of LmCld clashes with heme
- Figure 11:** LmCld crystal
- Figure 12:** Superposition of chain A of LmCld and NdCld
- Figure 13:** Superposition of LmCld and LmCld-protamine
- Figure 14:** Location of Ba²⁺ co-crystallized with LmCld contoured at 4 sigma
- Figure 15:** Heme-staining of native LmCld
- Figure 16:** X ray fluorescence spectra of NdCld, recombinant LmCld and native LmCld
- Figure 17:** ⁴⁸SO IgG negative control SEC-ICP-MS
- Figure 18:** ⁵⁶Fe trace of native LmCld SEC-ICP-MS
- Figure 19:** Plot of recorded m/z and their counts in the region of expected m/z of heme
- Figure 20:** TIC of native LmCld RP-nESI-MSMS
- Figure 21:** NdCld W145F superposed with wildtype NdCld
- Figure 22:** SLS profile of dimeric NwCld
- Figure 23:** SLS profile of pentameric apoNdCld
- Figure 24:** SLS profile of SsCld
- Figure 25:** UV-vis spectrum of SsCld
- Figure 26:** UV-vis spectrum of NdCld
- Figure 27:** Temperature- and pH-dependent catalase activity of SsCld

10. List of Tables

Table 1:	Antibiotics
Table 2:	Media, buffers and stock solutions
Table 3:	List of primers
Table 4:	PCR composition
Table 5:	PCR settings
Table 6:	Colony-PCR composition
Table 7:	Colony-PCR settings
Table 8:	List of constructs
Table 9:	Crystallization conditions
Table 10:	Stabilizing conditions of Additive Screen
Table 11:	Stabilizing conditions of Silver Bullets
Table 12:	Stabilizing conditions of Silver Bullets Bio
Table 13:	Data collection statistics of LmCld
Table 14:	Refinement statistics LmCld
Table 15:	Data collection statistics LmCld with protamine
Table 16:	Refinement statistics LmCld with Protamine
Table 17:	Contributions to anomalous scattering of barium and sulfur at 6200 keV
Table 18:	Data collection statistics of NdCld W145F
Table 19:	Refinement statistics of NdCld W145F
Table 20:	Data collection statistics of NdCld W145F with cyanide
Table 21:	Refinement statistics of NdCld W145F with cyanide
Table 22:	Comparison of steady-state kinetics of active Clds and mutants

11. Nomenclature

AEX	Anion exchange chromatography
AoCld	Chlorite dismutase from <i>Azospira oryzae</i>
AS	Additive Screen
Cld	Chlorite dismutase
DaCld	Chlorite dismutase from <i>Dechloromonas aromatica</i>
DMB	3',3'-dimethoxybenzidine
EDTA	Ethylendiaminetetraacetic acid
ESI	Electrospray ionization
Fc	Fragment crystallizable region of IgG
ICP-MS	Inductively coupled plasma mass spectrometry
IgG	Immunoglobulin G
IPTG	Isopropyl-beta-D-thiogalactopyranoside
k_{cat}	Turnover rate
K_{M}	Michaelis constant
LB	Lysogeny broth
LmCld	Chlorite dismutase from <i>Listeria monocytogenes</i>
LN ₂	Liquid nitrogen
m/z	Mass over charge ratio
NdCld	Chlorite dismutase from <i>Nitrospira defluvii</i>
nESI	nano Electrospray ionization
Ni-NTA	Nickel-nitriloacetic acid
NwCld	Chlorite dismutase from <i>Nitrobacter winogradskyi</i>
OD	Optical density
O/N	Over night
PCR	Polymerase chain reaction
PCRB	Perchlorate reducing bacteria
PerR	(Per)chlorate reductase
R_{free}	Cross-validation R-factor
R_{meas}	Redundancy-independent merging value (also called R_{rim})
R_{merge}	Linear merging value
RNAi	RNA interference
R_{work}	Linear residual fit between diffraction data and model
r.m.s.d.	Root mean square deviation
RP	Reverse phase
RZ	Reinheitszahl
SB	Silver Bullets
SBB	Silver Bullets Bio
SEC	Size exclusion chromatography
SLS	Static light scattering
SsCld	Chlorite dismutase from <i>Sulfolobus solfataricus</i>
TAE	Tris, acetic acid, EDTA buffer
TBE	Tris, boric acid, EDTA buffer

TCA	Trichloroacetic acid
TE	Tris, EDTA buffer
TBS	Tris-buffered saline
T _M	Melting temperature
TtCld	Chlorite dismutase from <i>Thermus thermophilus</i>
XRF	X-ray fluorescence

12. Acknowledgements

I want to thank everybody involved in my project, Kristina for providing a well functioning lab and the entire chlorite dismutase group: Kira, Julius, Georg, Christian, Paul, Stefan, Holger, Andrea and Christa. I would like to emphasize the importance of my tutors Georg, with whom it was always a pleasure talking about new developments in crystallography, Julius, who always had an open mind for my scientific problems and Kira, who introduced me to many methods used for this thesis. It was a pleasure working with you and letting your fascination infect me. Anita was always helpful with advice and action. Thanks to Claudia and every other member of my lab who supported me in data acquisition and processing. I would not have come this far without your help.

Thanks also to the NMR group for great coffee break conversations and barbecue, Stephanie Füreder for the marvelous antibodies, the groups of Christa Schleper, Thomas Decker and Stephan Hann.

Last but not least I want to thank my family and my girlfriend for supporting me throughout my studies.

Curriculum Vitae

Name	Andreas Hagmüller
Date of birth	May 21 st 1986
Place of birth	Wels, Austria
Nationality	Austrian

University

09/2005 – 03/2013 University of Vienna
Subject: Molecular Biology

Diploma thesis at the Department of Structural and Computational Biology, Max F. Perutz Laboratories, University of Vienna

Title: “Structural and Functional Characterization of Chlorite Dismutases and homologous proteins”

Supervised by Univ.-Prof. Dr. Kristina Djinovic-Carugo

Civil Service

09/2004 – 08/2005 Arbeiter Samriterbund Gruppe Bad Ischl

School

09/1996 – 07/2004 Bundesrealgymnasium Traun, Austria
Graduation with Matura 2004

09/1992 – 07/1996 Primary school St. Marien, Austria

Publications

Hofbauer S, Gysel K, Mlynek G, Kostan J, Hagmüller A, Daims H, Furtmüller PG, Djinovic-Carugo K, Obinger C. **“Impact of subunit and oligomeric structure on the thermal and conformational stability of chlorite dismutases.”** Biochimica et Biophysica Acta 2012 Sep;1824(9): 1031-1038

Hofbauer S, Bellei M, Sündermann A, Pirker KF, Hagmüller A, Mlynek g, Kostan J, Daims H, Furtmüller PG, Djinovic-Carugo K, Oostenbrink C, Battistuzzi G, Obinger C. **“Redox thermodynamics of high-spin and low-spin forms of chlorite dismutases with diverse subunit and oligomeric structures.”** Biochemistry 2012 Nov; 51(47): 9501-9512

Presentations at Conferences

15th Heart of European Bio-Crystallography Meeting, Beilngries, Germany 2012

“Chlorite Dismutase Family: Structural and Functional Characterization”